REVIEW ARTICLE | JANUARY 14 2026

Aerodynamic and aeroacoustic interactions in multirotor aircraft for urban air mobility: A review FREE

Kangni Combey ; Omer A. Elsayed ; Andrea Magrini ; Federico N. Ramirez ; Sen Wang ; Khaoula Qaissi ; Hajar Chouiyakh; Lourenço T. L. Pereira; Daniele Ragni

Physics of Fluids 38, 011303 (2026)
https://doi.org/10.1063/5.0311473

Aerodynamic and aeroacoustic interactions in multirotor aircraft for urban air mobility: A review

Cite as: Phys. Fluids **38**, 011303 (2026); doi: 10.1063/5.0311473
Submitted: 10 November 2025 · Accepted: 23 December 2025 ·
Published Online: 14 January 2026

View Online Export Citation CrossMark

Kangni Combey,[1,a] Omer A. Elsayed,[1] Andrea Magrini,[2,a] Federico N. Ramirez,[3] Sen Wang,[4] Khaoula Qaissi,[1] Hajar Chouiyakh,[1] Lourenço T. L. Pereira,[4] and Daniele Ragni[4]

AFFILIATIONS

[1]School of Aerospace and Automotive Engineering, International University of Rabat, 11100 Sala Al Jadida, Morocco
[2]Dipartimento di Ingegneria Industriale, Università Degli Studi di Padova, Via Venezia 1, 35131 Padova, Italy
[3]CMT – Clean Mobility & Thermofluids, Universitat Politècnica de València, Camino de Vera, 46022 Valencia, Spain
[4]Flow Physics and Technology Department, Delft University of Technology, 2629 HS Delft, The Netherlands

[a)]Authors to whom correspondence should be addressed: kangni.combey@uir.ac.ma and andrea.magrini@unipd.it

ABSTRACT

The rapid growth of urbanization and increasing road traffic congestion are straining ground transportation infrastructure for both conventional and emergency purposes, driving the need for alternative mobility solutions. urban air mobility (UAM) offers a promising pathway by deploying electric vertical takeoff and landing (eVTOL) aircraft to enable efficient and flexible aerial transport in dense urban environments. However, the successful integration of UAM into city airspace faces critical technical challenges, both at the vehicle and operational levels. In particular, complex aerodynamic and aeroacoustic interactions between closely spaced propellers significantly influence vehicle performance, energy efficiency, and public acceptance. This work presents a review of experimental and computational studies on propeller–propeller and propeller–wing interactions, highlighting the state-of-the-art methodologies and their application to multirotor eVTOL designs. Results indicate that distributed electric propulsion systems arranged in side-by-side configurations exhibit minimal thrust degradation, typically less than 3% compared to an isolated propeller. However, reductions in propeller spacing can induce unsteady blade loading and increase tonal noise levels by up to 10 dB. In contrast, one-after-another configurations may suffer thrust losses of up to 80%, due to slipstream ingestion by the rear propeller, with a lateral separation of at least twice the propeller radius required to recover performance within 4% of the isolated case. The review also addresses propeller–wing interactions that modify local pressure distributions and spanwise lift, particularly in wing-mounted distributed propulsion configurations. The insights provided establish a foundation for developing efficient, low-noise multirotor architectures for future UAM integration.

I. INTRODUCTION

The concept of urban air mobility (UAM) represents a significant evolution in the transportation of people and goods. By employing electric vertical takeoff and landing (eVTOL) aircraft, UAM envisions a future where these aircraft, commonly referred to as "air taxis" or "flying cars," are seamlessly integrated into urban airspace, providing a novel mode of transportation for both intercity and intracity travel. Figure 1 illustrates an example of urban air transportation. In Fig. 1(a), concept vehicles are depicted flying over an urban area, traveling between multiple locations.[1] Figure 1(b) shows an urban air mobility eVTOL aircraft from Eve Air Mobility, illustrating the passenger seating arrangement.[2]

This innovation aims to alleviate ground traffic congestion and reduce travel times, while also minimizing noise emissions and the costs associated with the larger payload and landing footprint typical of conventional air vehicles. For example, an estimation by Uber Elevate indicates that travel from San Francisco to San Jose could be reduced to approximately 15 min by air taxi, compared to the usual 1 h and 40 min by ground car transportation.[3] Additionally, UAM is expected to help address climate change concerns by adopting electric propulsion systems, delocalizing the direct emissions in the most populated urban transportation networks, and improving accessibility to previously difficult-to-reach areas, including remote and mountainous regions.[4–6]

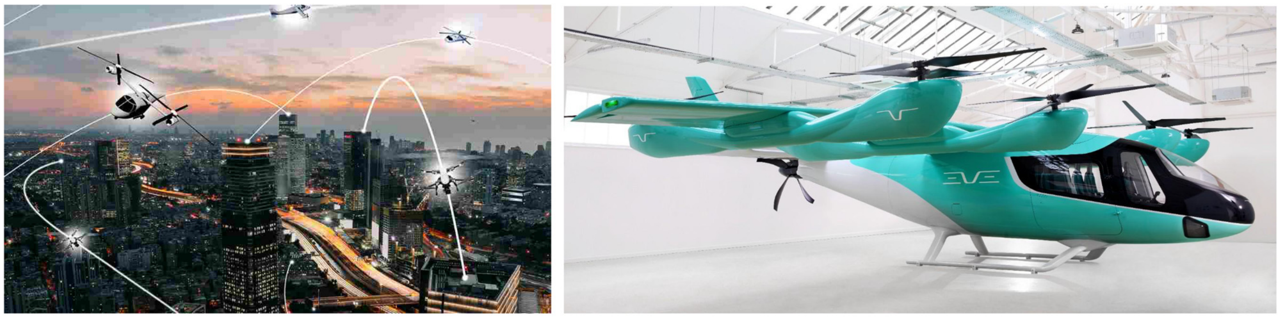

(a) (b)

FIG. 1. UAM. (a) Urban air transportation (image courtesy of NASA, public domain).[1] (b) Eve Air Mobility eVTOL aircraft (image Copyright Eve Air Mobility, used with permission).[2]

To address growing challenges related to congestion and climate impact, many urban areas are turning to sustainable ground-based transport such as shared mobility, rail, and bus services. However, in densely populated cities with constrained infrastructure and road complexity, these terrestrial systems may not be sufficient to meet all critical mobility needs, particularly for time-sensitive services such as emergency response. For instance, a recent study revealed that ambulance response times in some Dutch cities have increasingly failed to meet urgent service thresholds due to traffic delays.[7] Hence, eVTOLs stand as an attractive solution for urban mobility.

UAM is poised to introduce diverse services, ranging from emergency transportation to delivery logistics, integrating both manned and unmanned aerial vehicle functionalities.[8] Key applications include on-demand passenger and cargo services, spanning shared air taxis to private ownership models and emergency response,[9,10] where UAM can significantly reduce medical response times (e.g., from 21 to 7–9 min in Paris),[11,12] as well as support disaster relief operations. Additionally, UAM enhances logistics efficiency by enabling rapid goods delivery through autonomous drones.[13–16] Consequently, cities can improve their emergency response and accelerate service delivery by leveraging the agility and versatility of eVTOL aircraft.

Beyond transportation, UAM technologies serve diverse roles including aerial cinematography, night operations, and surveillance, demonstrating broad potential across urban and specialized environments. Recognizing this, stakeholders from aeronautics, ground transportation, aerospace startups, and policymakers are actively collaborating to realize UAM concepts.[17–20] Moreover, UAM requires minimal infrastructure, consisting only of start and end points called vertiports[21] or vertidromes.[22]

The technical realization of UAM relies heavily on distributed electric propulsion (DEP), which employs multiple low-disk-loading rotors or propellers to enhance safety, noise reduction, and operational efficiency.[23–26] Advances in high-performance electric motors, with high power-to-weight ratios, scalability, reliability, and digital control systems, allow independent, real-time thrust modulation across propellers, eliminating mechanical complexities such as gearboxes and swash-plate systems.[27–30] The multirotor architecture inherently provides redundancy, improving stability and fault tolerance, while enabling precise pose control[31] and expanding aerodynamic design possibilities suited for urban environments. DEP also contributes to reduced noise and enhanced propulsive efficiency by replacing mechanically complex components with quieter electric drives and using multiple smaller propellers strategically placed, often on the suction side of lifting surfaces, to increase lift at low speeds.[32] Furthermore, smaller propellers reduce structural risks during incidental contact with urban infrastructure, improving operational safety and reliability in densely populated areas.[23,33]

However, this distributed approach introduces new aerodynamics and acoustics challenges.[34,35] In order to remain compact and meet weight and thrust requirements, eVTOLs often place propellers in close proximity, leading to significant propeller–propeller and propeller–airframe interactions. These interactions can reduce thrust efficiency, increase unsteady loading, and noise emissions, which play a crucial role in community acceptance. UAM vehicles are expected to operate in noise-sensitive environments and perform frequent takeoffs and landings. Therefore, understanding how propeller proximity and layout influence both tonal and broadband noise is essential for regulatory compliance and public acceptance. Despite the promise of electric propulsion in reducing vehicle noise, rotating blades and aerodynamics interactions can still generate high-amplitude, low-frequency signatures that propagate far in urban areas.

Moreover, the transition between vertical and forward flight phases introduces additional complexity. Tiltrotor and tilt-wing architectures expose propellers to non-axial inflow, leading to azimuthally varying blade loading,[36] unsteady thrust, and changes in wake structure. These effects are further intensified when multiple propellers interact within a single flow field, creating phenomena not typically encountered in conventional rotorcraft or fixed-wing aircraft.

Although recent studies have addressed individual aspects of eVTOL vehicle performance, a comprehensive synthesis of aerodynamic and aeroacoustic interactions in multirotor UAM configurations remains limited. Multiple interaction types exist, including propeller–propeller, propeller–lifting surface, propeller–fuselage, and propeller–non-lifting arm interactions. Each can alter local flow structures, reduce efficiency, and increase radiated noise. Nearby components affect propeller flow, while the propeller simultaneously modifies the flow around them; however, not all mechanisms contribute equally to overall performance degradation. For instance, Li *et al.*[37] showed that fuselage-induced effects in wingless multirotor configurations are relatively minor compared with the strong aerodynamic and acoustic coupling from propeller–propeller interactions. Accordingly, this review focuses on the two interactions most consistently identified as dominant, specifically propeller–propeller and propeller–wing interactions. Emphasis is placed on the effects of propeller spacing in typical side-by-side (SBS) and one-after-another (OAA) configurations, as well as propeller placement relative to the lifting surface (wing).

This work consolidates the current state of the art in experimental measurements, computational fluid dynamics (CFD), and computational aeroacoustics (CAA) as applied to aerodynamics and aeroacoustics interaction phenomena. It further aims to provide practical guidance for the aerodynamic and acoustic design of UAM vehicles, thereby supporting their effective integration into future urban transportation networks.

Throughout this paper, the term *multirotor* refers to configurations employing multiple rotors or propellers within distributed electric propulsion (DEP) systems. The term *propeller* is used generically to describe both vertically and horizontally oriented propulsion units, unless otherwise specified. The term *rotor* is reserved for vertical-lift units operating in a fixed orientation, as commonly found in multicopter architectures. The term *tiltrotor* refers specifically to propulsion systems capable of transitioning between vertical (hover) and horizontal (cruise) orientations, typically through mechanical tilting mechanisms.

The remainder of this paper is organized as follows: Sec. II presents representative configurations of UAM vehicles and propulsion system layouts and discusses key challenges related to community acceptance, propeller integration, and aerodynamic and aeroacoustic performance. Section III examines the aerodynamic behavior of multirotor systems, including single-propeller performance, propeller–propeller interactions in various configurations, and propeller–wing interactions. Section IV presents the corresponding aeroacoustic phenomena associated with these configurations. Section V summarizes the implications of aerodynamic and aeroacoustic interactions for UAM vehicle design. Finally, Sec. VI provides concluding remarks and future research directions.

II. UAM VEHICLES CONFIGURATIONS AND CHALLENGES

Urban air mobility vehicles are designed to operate within densely populated environments, typically at low altitudes, typically around 4000 ft (1.2 km),[38] as illustrated in Fig. 2. Consequently, eVTOL aircraft have predominantly adopted propeller-driven propulsion systems. These systems offer a favorable balance of aerodynamic efficiency, mechanical simplicity, and scalability at lower speeds and altitudes.[39]

A distinctive feature of many eVTOL configurations is the dual functionality of their rotating blades. Unlike conventional fixed-wing aircraft, eVTOL vehicles use thrust-generating devices that operate as rotors and/or propellers, depending on the flight regime.[40] During vertical takeoff and landing phases, these rotors primarily generate vertical lift to support the weight of the aircraft. In forward flight, their role transitions to that of propellers, generating horizontal thrust to overcome drag. As the aircraft gains speed, aerodynamic surfaces, such as wings, begin to contribute significantly to lift, enabling more efficient cruise performance, particularly in winged configurations. This transition between vertical and horizontal flight imposes unique demands on both propulsion and control architectures. The need for compactness, system redundancy, and a reduced noise footprint further influences vehicle configuration, often leading to multirotor designs.

UAM aircraft are expected to operate in close proximity to people and infrastructure, such as buildings and towers. As such, they must maintain minimal takeoff and landing footprints, unlike conventional air vehicles. This requirement necessitates compact designs that can still accommodate a variety of mission profiles (see Fig. 3), ranging from short- to medium-range (50–100 km) flights for intracity transport to longer-range (100–300+ km) operations for intercity travel.[41] To meet power and redundancy requirements within these compact airframes, UAM vehicles typically incorporate multiple propulsive units distributed across the airframe. These propulsion systems are commonly arranged in tightly packed configurations, with propellers placed in close proximity.

This section reviews representative UAM vehicle architectures, emphasizing propulsion layout and the key challenges posed in terms of aerodynamics and acoustics.

A. Classification of UAM vehicles concepts

A key distinction among eVTOL configurations lies in their methods of generating lift and thrust. Fixed-wing designs produce aerodynamic lift through forward motion and pressure differentials

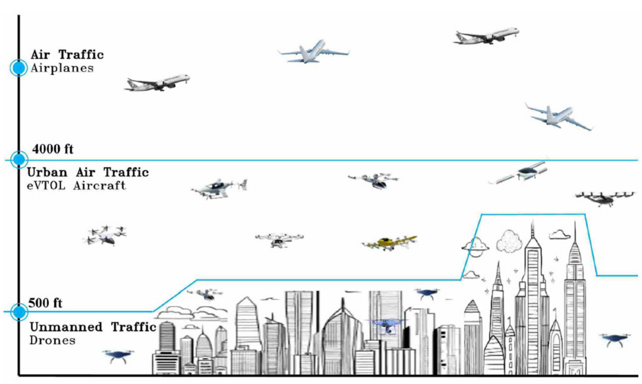

FIG. 2. Airspace showing the urban air traffic region below 4000 ft (1.2 km).

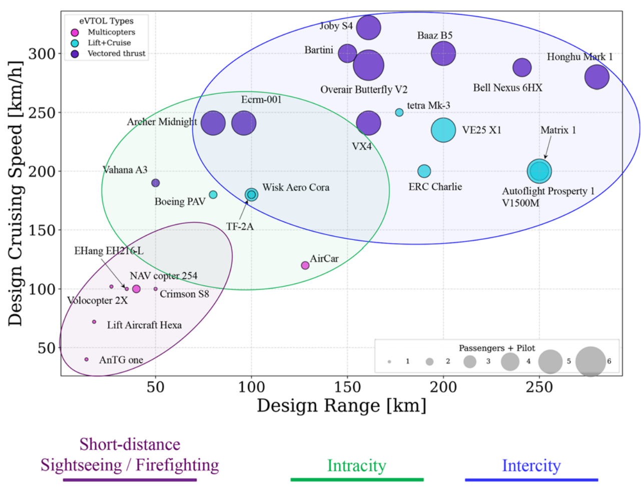

FIG. 3. Design cruise speed vs design range for UAM eVTOL aircraft.

over wings,[42] while rotor-based systems generate lift by accelerating air downward via rotating blades.[43]

These mechanisms result in notable differences in aerodynamic efficiency. Fixed-wing UAVs typically achieve cruise lift-to-drag (L/D) ratios between 10 and 20, depending on design and mission.[44–47] For instance, Qiao *et al.*[48] reported an L/D of 10.4 for a micro-UAV. In contrast, rotorcraft have lower cruise efficiency due to higher drag and lack of lifting surfaces.[49,50] Their hover efficiency is often quantified by the figure of merit (FoM), typically ranging from 0.4 to 0.8.[51–53]

With growing UAM demand, the number of eVTOL concepts has surged from a few in 2017 to over a thousand today.[54] These designs are generally categorized into four types based on thrust generation: vectored thrust, lift + cruise, wingless (multicopter), and electric rotorcraft (eHelos).[50,54,55]

1. Vectored thrust

This concept entails an eVTOL aircraft that can lift and cruise using all of its thrusters, i.e., there is no distinction between thrusters deployed for each flight phase. Thrust vectoring is achieved through either tilt-wing or tiltrotor configurations.[50,56] In tilt-wing designs, propellers are mounted on a wing that rotates as a unit to modify the thrust direction. This configuration enables vertical takeoff and landing, while allowing high cruise performance due to propeller alignment with the flight direction.[56,57] Notable examples include the Aurora Lightning Strike[58] and the Airbus A^3 Vahana.[59] The Vahana was initially expected to achieve a cruise speed of 230 km/h with a range of 100 km;[54] however, the demonstrated performance included a range of approximately 50 km at cruise speed between 185 and 190 km/h for a flight duration of up to 20 min.[59,60] In contrast, tiltrotor designs feature propellers that independently pivot relative to fixed wing or non-lifting surfaces, rather than tilting the entire wing structure. Representative aircraft in this category include the Joby S4[61] and Bell Nexus.[62] The Joby S4 is designed for a cruise speed of 322 km/h and a range of 161 km.[60] It has been reported an estimated lift-to-drag (L/D) ratio ranging from 12.5 to 14.3, depending on operating conditions.[46,63,64] The measured noise level at a cruise speed of 185 km/h and an altitude of 500 m is 45.2 dBA, increasing to 65 dBA at a distance of 100 m from the ground,[61] indicating that the aircraft operates with relatively low noise emissions.

The primary advantages of vectored thrust configurations, both tilt-wing and tiltrotor, include the ability to achieve higher cruise speeds and higher aerodynamic performance, primarily due to better thrust alignment during forward flight and favorable disk loading characteristics. However, it incorporates complex mechanism due to the tilting of propellers. The addition of tilting mechanism also adds weight to the vehicle, which compromises the maximum payload.

2. Lift + cruise

The second category of eVTOLs is known as lift + cruise (L+C). These aircraft, such as the Kitty Hawk Cora[65] and the Beta Technologies ALIA-250,[66] also feature fixed wings for efficient cruising. Nevertheless, unlike vectored thrust eVTOLs, lift + cruise designs use separate propulsion systems for hovering and cruising, eliminating the need for thrust vectoring.[67–69] Typically, these eVTOLs deploy fixed vertical rotors for hover and horizontal propellers to generate the required forward thrust during cruise flight. For instance, the ALIA-250 is designed to achieve top cruise speed of 250 km/h,[66] with a maximum range of 500 km.[54] This dual propulsion system allows for efficient vertical takeoff and landing as well as simplified mechanical architecture. However, the presence of lift rotors during cruise introduces additional parasitic drag, thereby reducing the effective L/D ratio[64,70] compared to the vectored thrust. Bacchini *et al.*,[71] using a Mini Talon UAV model, demonstrated experimentally that the maximum L/D decreases from 16 to 12 when lift motors and propellers are integrated into the wing for cruise flight, and further declines to 9 when the propellers are oriented perpendicular to the freestream. These results highlight that lift motors and propellers are the primary sources of drag in lift + cruise configurations during forward flight. Therefore, retracting or aerodynamically fairing the lift propulsion system is essential to reduce drag and enhance cruise efficiency in small-scale lift + cruise drones. However, for passenger-carrying eVTOL vehicles, these strategies may offer limited benefits. Retraction mechanisms or large fairings require additional structural volume, which can increase the total wetted area and potentially lead to higher overall drag during cruise. It is possible to have a lift+lift/cruise (L+L/C) configuration, such as the Vertical VX4,[72] in which some propellers are dedicated to lift only, while others tilt to provide both lift and cruise thrust.

3. Wingless

Wingless eVTOLs, such as the EHang 216[73] and the Volocopter Velocity 2X,[74] are multirotor aircraft that lack dedicated cruise thrusters and rely exclusively on lift rotors for both hovering and forward flight.[55,75] This configuration provides a large total disk area and improves hover performance. However, the absence of wings limits their aerodynamic performance during cruise flight, which leads to greater energy consumption compared to those with wings. Reported cruise speeds are typically limited to 90–100 km/h, with maximum ranges of approximately 30–35 km.[60,73,74] Furthermore, the effective L/D in cruise is estimated to remain below 5,[49,64,70,76] similar to that of conventional helicopters.[43] Consequently, these eVTOLs are best suited for short-range, intra-city missions and can operate efficiently within urban air corridors.

4. eHelos

Electrically powered rotorcraft, often referred to as electric helicopters or eHelos, are conventional rotorcraft configurations utilizing electric propulsion systems. These aircraft employ a main rotor system for both lift and propulsion, akin to traditional helicopters or autogyros.[50] In the case of autogyros, the main rotor operates in autorotation, generating lift without direct power input, and continues to rotate in the event of engine failure, thereby helping in controlled descent. Examples within this category include the Aquinea Volta[77] and the Skyworks eGyro.[54] The Skyworks eGyro has been reported to target cruise speeds ranging from 161 to 241 km/h.[54] eHelos vehicles are more applicable for specific use cases than high-density UAM operations.

Summary of most design concepts employed on current UAM vehicles are summarized in Table I. Each eVTOL configuration presents unique advantages and limitations, with the optimal design contingent upon the intended mission profile. As illustrated in Fig. 3, wingless configurations are generally suitable for short- to medium-range (intracity)

TABLE I. Comparison of different UAM vehicle types and their characteristics.

Vehicle	Configuration	Key characteristics	Examples	Range (km)
Vectored thrust	Tilting rotors/propellers or tilting wing for lift/thrust	High cruise speed and range; capable hover performance; complex mechanical systems	Vahana, Joby S4	50–300+
Lift + cruise	Separate propellers for lift and forward propulsion	Balances hover efficiency with moderate cruise performance; simpler than vectored thrust systems	Beta ALIA, EHang VT-30	50–250
Multicopter (lift only)	Multiple vertical fixed rotors	Efficient in hover; poor aerodynamic efficiency in cruise flight; lower range	Volocopter, EHang	0–50

missions, including passenger transport and tasks such as agriculture, urban firefighting, and aerial tourism. In contrast, lift + cruise and vectored thrust configurations are better aligned with medium- to long-range (intra- and intercity) operations due to their superior aerodynamic efficiency and cruise performance.

B. Impact of noise on community acceptance

Commercial aircraft generate substantial noise during operation, particularly during takeoff and landing phases; however, flyover noise can also be a source of annoyance. To mitigate community exposure, regulatory noise limits are enforced in the vicinity of airports. Noise levels can be measured using Weighted Equivalent Continuous Perceived Noise Levels (WECPNL),[78] which accounts for both peak noise levels and time-of-day weighting factors.

Table II, summarizes the impact of WECPNL in the cities as presented by Kim *et al.*[79] Noise levels around 90 dBA are typically associated with helicopters, while levels exceeding 100 dBA are common for larger airplanes. In this classification, noise levels above 90 dBA are deemed extremely disruptive and unsuitable for residential areas, whereas levels below 70 dBA are considered comfortable for living. However, considering hundreds of urban air vehicles operating at noise levels up to 70 dBA, and repetitively, this will still be loud and the cumulative effect can still be disruptive.

Although dedicated noise certification standards for urban air mobility (UAM) vehicles are still under development by regulatory authorities such as the Federal Aviation Administration (FAA)[80] and the European Union Aviation Safety Agency (EASA),[81] existing standards for tiltrotor aircraft provide a relevant baseline. For instance, FAA 14 CFR Part 36, Appendix K,[82] defines Effective Perceived Noise Level (EPNL) limits as a function of maximum gross weight. This suggests that for tiltrotors in the 2000–4000 kg weight class, representative of current UAM designs such as Joby S4 (2404 kg[54]) and Archer Midnight (3175 kg[54]) expected allowable EPNL values range from approximately 92 to 97 EPNdB under flyover, takeoff, and approach conditions (see Fig. 4). While these thresholds may be suitable for conventional tiltrotors, they are considerably high for UAM vehicles, which are expected to operate at low altitudes in densely populated urban environments with frequent takeoffs and landings. This emphasizes the need for dedicated evaluation and certification pathways tailored to eVTOL configurations.

TABLE II. Effect of aircraft noise on the cities. Data from Ref. 79.

WECPNL	Loudness	Effects on a residential environment
≥ 90	Very noisy	Difficult to live
$80-89$	Noisy	Requires the installation of soundproofing for residential buildings
$76-79$	Slightly noisy	Requires the installation of soundproofing for schools and hospitals
$71-75$	Not noisy	Sufficient for living
≤ 70	Not noisy at all	Comfortable for living

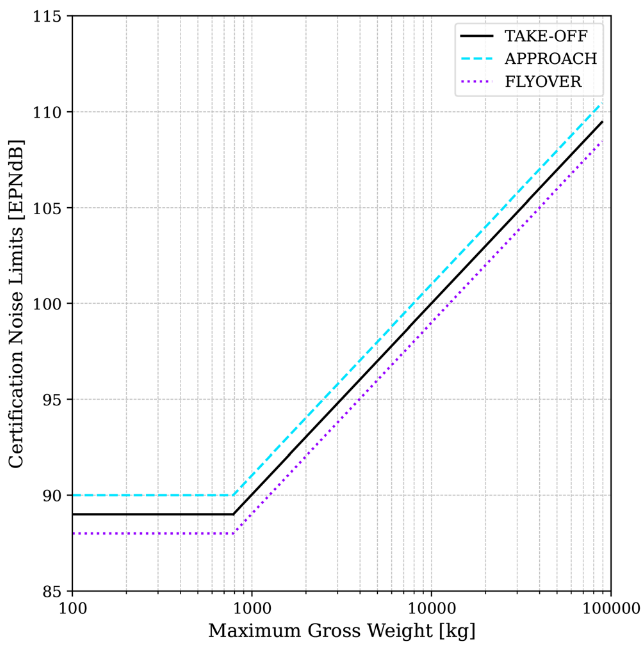

FIG. 4. Tiltrotor noise limits. Data extracted from Ref. 82.

In response to this need, regulatory authorities have introduced interim frameworks, including the FAA Special Federal Aviation Regulations (SFAR) and EASA Special Condition for VTOL (SC-VTOL), for current UAM vehicles. The FAA has issued Powered-Lift Notices of Proposed Rulemaking (NPRMs), which recognize that existing standards are insufficient for emerging eVTOL configurations and allow noise evaluations on a case-by-case basis until dedicated standards are finalized.[83] In Europe, EASA's SC-VTOL provides the primary airworthiness framework, and ongoing Means of Compliance (MOC) publications extend guidance relevant to noise assessment.[84] Recent research, including NASA studies and community-noise investigations, underscores the critical role of psychoacoustic metrics such as loudness, sharpness, tonality, roughness, and fluctuation strength in quantifying perceived annoyance in urban environments. These sound-quality metrics (SQMs) correlate more reliably with human response than conventional sound-pressure levels and are anticipated to play a central role in shaping future noise-certification frameworks for urban air mobility vehicles.[85–87]

To minimize community noise impact, NASA researchers[89] recommend that UAM vehicles target noise levels substantially lower than those of conventional rotorcraft, noting that noise levels above 65 dBA, are associated with community annoyance. Industry guidance from Uber Elevate suggests that VTOL vehicles should aim for A-weighted noise levels not exceeding 62 dBA at an altitude of 500 ft (152 m).[3] Furthermore, based on environmental-noise guidelines, stricter targets around 55 dBA or lower are advised for early morning and late evening hours, when background noise is minimal and public sensitivity is higher.[90] These baselines provide guidance for UAM vehicle design and operations to reduce perceived annoyance and enhance community acceptance.

Table III presents typical noise levels of current UAM vehicles. Many eVTOL concepts only specify target noise levels above 60 dBA, as they have not yet been tested under real operating conditions. Some leading developers, such as Joby Aviation, have reported actual measured noise levels based on NASA testing; for example, the Joby S4 produces 45.2 dBA during a flyover at 500 m altitude and 65 dBA at 100 m.[54] Near the ground, noise levels are higher. Casalino *et al.*[88] conducted a study on community noise in urban air transportation at 1 m above the ground and reported overall sound pressure levels (OASPL, in dB) exceeding 65 dB for three different approach maneuvers (see Fig. 5), highlighting the difficulty of maintaining target low noise levels.

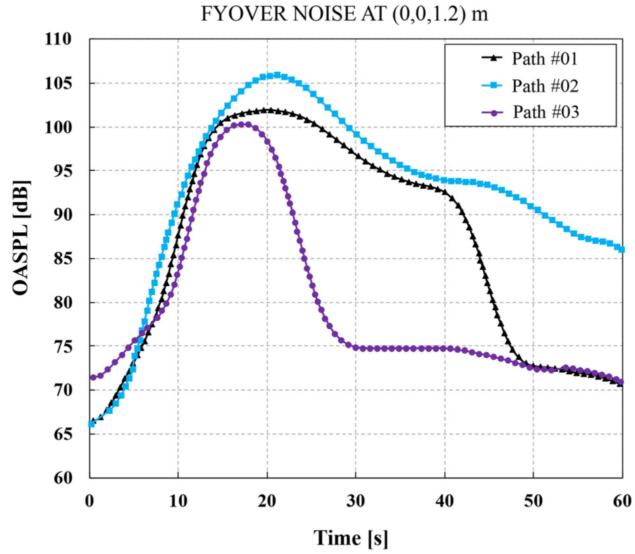

FIG. 5. UAM OASPL over time for three different approaching trajectories. Data extracted from Ref. 88.

C. Propeller configurations in compact UAM vehicles

The defining characteristic of DEP-based eVTOLs is the spatial arrangement of multiple propellers, and from the above presented configurations, the arrangements can be grouped into two primary configurations that dominate.

In one-after-another (OAA) configuration, propellers are axially aligned (co-axial) along the same thrust column,[35] enabling compact longitudinal stacking without increasing the lateral footprint of the vehicle, an important consideration for urban operations [see Fig. 6(a)]. This configuration supports redundancy by allowing inline integration of backup propellers and offers additional control authority through differential thrust for pitch and transition maneuvering. However, the downstream propeller operates in the wake of the upstream propeller, experiencing highly non-uniform inflow characterized by swirl and slipstream ingestion.[93] This leads to degraded aerodynamic performance, increased unsteady blade loading, and therefore the overall noise level due to the interactions.

In side-by-side (SBS) configuration, propellers are placed laterally adjacent in the same plane (co-planar),[94] offering uniform lift distribution and effective yaw and roll control via differential thrust [see Fig. 6(b)]. However, SBS configurations designed for efficient cruise may increase the lateral footprint of the vehicle when mounted on the

TABLE III. Noise levels of selected current UAM vehicles.

UAM vehicle	Noise level (dBA)
EHang 216	100 (target at 30.5 m)[79]
CityAirbus	70 (target)[91]
Bell Nexus	67 (target)[79]
Hyundai S-A1	60 (target)[79]
Joby S4	45.2 at 500 m/65 at 100 m[92]

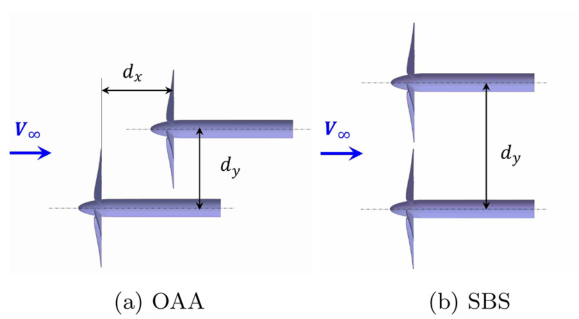

FIG. 6. Typical multirotor configurations.

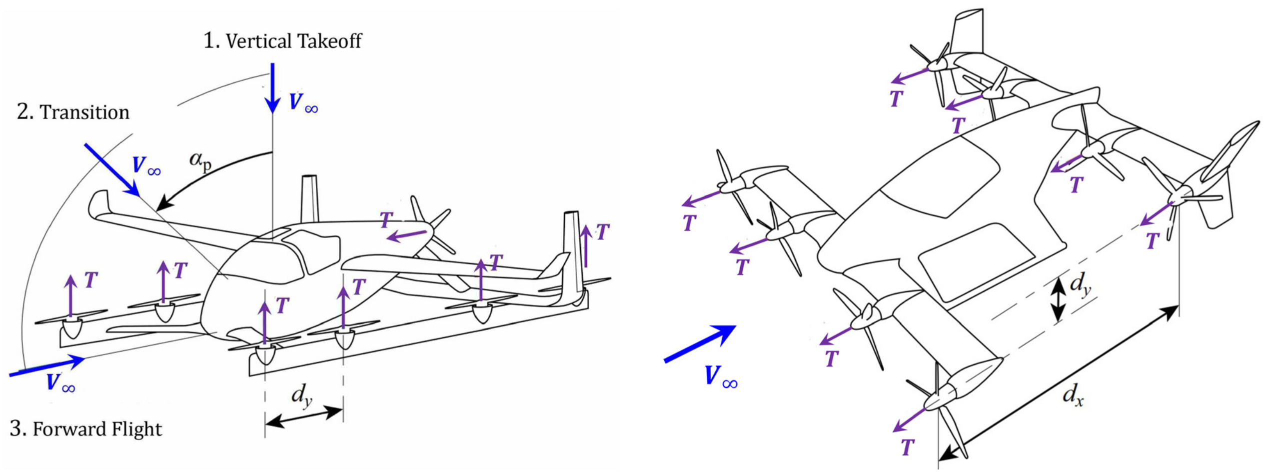

(a) Aurora Passenger vehicle with SBS propellers (b) Airbus Vahana vehicle with OAA propellers

FIG. 7. eVTOL vehicles showing propellers in SBS and OAA configurations: (a) Aurora passenger vehicle with SBS propellers; (b) Airbus Vahana vehicle with OAA propellers. Reproduced with permission from Stokkermans *et al.*[35] Copyright 2021 by the authors.

wings, which can limit compact airframe designs, especially for urban operations. Nevertheless, it is possible to integrate SBS propellers into a compact multicopter design by mounting them on arms, as shown in Fig. 7(a). When spacing between propellers is reduced, aerodynamic interference can occur, leading to unsteady loading, and increase tonal noise level due to the interactions between the propellers.[95]

In practice, most UAM eVTOL with high thrust-to-weight demands and constrained airframe dimensions employ a SBS and OAA propeller configuration. As shown in Fig. 7(b), SBS propellers may be distributed along lateral lifting booms, while OAA propellers are positioned at the tail or aft section to provide pitch control and redundancy. This hybrid configuration allows designers to leverage the advantages of both layouts, namely, compact arrangement, efficient vertical lift, and enhanced control authority, without substantially increasing the footprint of the vehicle, a critical consideration for urban constraints.

However, the coexistence of SBS and OAA configurations introduces additional aerodynamic complexity. Each propeller experiences a distinct flow environment based on its position and operating condition, complicating performance prediction, noise modeling, and control system design. Interactions between propellers, wings, fuselage elements, and non-lifting structures become highly coupled, particularly during transition phases or in gusty urban environments.

Both SBS and OAA arrangements present unique aerodynamic and acoustic trade-offs, impacting propulsive efficiency, and community noise exposure. Optimal performance requires careful propeller spacing, phase management, and integration strategies to mitigate unsteady loading and tonal noise. The hybrid design enables improved thrust distribution and maneuverability without compromising footprint, but demands a more holistic aerodynamic and acoustic design framework.

D. Aerodynamics and aeroacoustics challenges

Given the promising operational and environmental benefits of eVTOL aircraft, their widespread adoption depends on overcoming a range of challenges, as shown in Fig. 8. These include technical challenges, regulatory requirements, and public acceptance. The successful implementation of UAM vehicles in urban areas is contingent upon addressing all three of these critical dimensions.

This work focuses on the technical dimension of eVTOL vehicle design, with particular attention to how compact multirotor configurations influence aerodynamic performance and noise generation. The highly integrated nature of eVTOL architectures, where lifting and propulsive systems often share tight spatial constraints, introduces complex flow phenomena and exacerbates aerodynamic interference effects. These effects are especially significant in configurations employing multiple propellers, tilt mechanisms, or combining lift and cruise functionalities, where the interactions between flow structures degrade aerodynamic performance and increase unsteadiness.

In such vehicles, several forms of aerodynamic interference must be considered, including: propeller–propeller interactions, propeller–wing

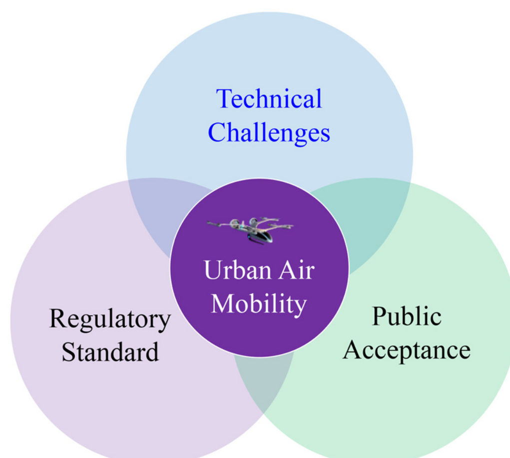

FIG. 8. UAM vehicles implementation challenges.

interactions, propeller–fuselage and propeller–non-lifting components interactions. Among these, the most significant are propeller–propeller and propeller–wing interactions[37] due to their direct impact on thrust production, stability, and control of the vehicle. In closely spaced multirotor systems, propeller–propeller interaction arises when a propeller operates within the slipstream of another. The downstream propeller experiences a disturbed, non-uniform inflow field that reduces local dynamic pressure and alters the effective angle of attack along the blades. This condition decreases its thrust generation capability, potentially requiring higher rotational speeds to compensate, at the cost of greater power consumption and reduced energy efficiency.[35,93,96]

Similarly, propeller–wing interaction occurs when propeller wakes impinge on adjacent lifting surfaces.[97] These interactions distort pressure distributions, influence boundary layer behavior, and can induce local flow separation or reattachment. Such flow distortions can improve or degrade lift generation and contribute to loading fluctuation. These effects are more intensified during non-axial inflow conditions.

These aerodynamic phenomena are intrinsically linked to aeroacoustic challenges.[98] Aerodynamics interaction, unsteady loading, and inflow distortion lead to fluctuating surface pressure distributions, which are primary sources of noise emission. Specifically, the propeller blades act as dipole sources, with tonal noise arising from periodic interactions, such as blade–wake and blade–blade interactions and broadband noise stemming from turbulence, vortex shedding, and flow separation.

In compact multirotor configurations, the proximity of multiple propellers can lead to constructive acoustic interference, where the sound waves from individual sources align and amplify, creating increased noise levels in specific directions. Furthermore, when propellers operate in non-axial flow as in forward flight or during the transition phase, azimuthal loading becomes asymmetric and time-periodic.[99] These oscillating loads generate more complex and intense acoustic fields, contributing to higher noise intensity.

The resulting acoustic signature poses a significant barrier to UAM deployment in noise-sensitive environments. Target sound pressure levels (SPLs), such as 62 dBA at 500 ft altitude,[3] or lower thresholds around 55 dBA,[100] have been proposed to ensure community acceptance. Meeting these targets is particularly challenging given that each rotating blade is itself a noise source, and the cumulative effect of multiple propellers can lead to unacceptable noise levels without careful aerodynamic and acoustic design.

Thus, the aerodynamic and aeroacoustic challenges of multirotor eVTOL systems are deeply interrelated. Propeller–propeller and propeller–wing interactions not only reduce thrust and efficiency but also intensify noise generation through increased unsteadiness and pressure fluctuation. These dual effects underscore the necessity for integrated design methodologies that consider aerodynamic performance and noise generation concurrently rather than sequentially.

This review aims to systematically examine the current understanding of these interaction effects, focusing particularly on propeller–propeller and propeller–wing interactions, identified as the most dominant and performance-critical. By synthesizing recent findings from both computational and experimental studies, the goal is to support the development of low-noise, high-efficiency eVTOL designs that are suitable for safe, quiet, and sustainable UAM operation.

III. MULTIROTOR AERODYNAMICS

Multirotor eVTOL aircraft generate thrust through multiple propellers or rotors. The thrust produced must balance the weight of the aircraft in order for it to hover and give additional thrust for vertical takeoff and cruising. The concepts of lift and thrust generation in multirotors are drawn from traditional helicopter and propeller aerodynamics.[43,101,102] The presence of several rotors results in more complex interactions. To understand the effects of the multirotor aerodynamic interaction on the propeller loading, first the aerodynamics of an isolated propeller is introduced.

A. Single propeller aerodynamics

The propeller blade operates as a rotating aerodynamic surface, employing mechanical torque to generate aerodynamic thrust. The thrust generated by the propeller results from a pressure differential across the blade surfaces, with higher pressure on the upstream side and lower pressure on the downstream side. This pressure differential induces a momentum change in the fluid, counteracting the aerodynamic forces exerted on the blades. The propeller generates thrust by displacing and accelerating the air rearward, producing a slipstream characterized by complex flow patterns, including turbulence and high swirl velocities.

As shown in Fig. 9(a), the slipstream consists of a vortex system with tip- and root-vortices for each blade, which creates induces velocity components. From momentum theory, half of the axial velocity increases in front of the propeller disk and the second half in the far downstream.[103] This results in the contraction of the streamtube due to conservation of the mass flow rate.[104,105]

In Fig. 9(b), the velocity diagram at a blade section located at radial position r is illustrated. The blade section, inclined at a local pitch angle β, encounters a relative velocity V_R. This relative velocity results from the combination of the freestream velocity V_∞, the rotational velocity ωr, the induced axial velocity $V_{a_i} = aV_\infty$, and the induced tangential velocity $V_{t_i} = a'\omega r$, where $\omega = 2\pi n$. This generates an elemental resultant force dF_R, which consists of the sectional thrust dT and the tangential force dF_Q. These forces can also be decomposed into sectional lift dL and drag dD. Integrating the elemental thrust and torque over the entire blade span, from hub to tip, and multiplying by the number of blades B, gives the total propeller thrust T and torque Q.

The propeller performance metrics are generally specified in terms of non-dimensional quantities such as advance ratio J, thrust coefficient C_T, torque coefficient C_Q, power coefficient C_P, and propulsive efficiency η_p or figure of merit FoM as defined by

$$J = \frac{V_\infty}{nD_p}, \tag{1}$$

$$C_T = \frac{T}{\rho_\infty n^2 D_p^4}, \tag{2}$$

$$C_Q = \frac{Q}{\rho_\infty n^3 D_p^4}, \tag{3}$$

$$C_P = \frac{P}{\rho_\infty n^3 D_p^5} = 2\pi C_Q, \tag{4}$$

$$\eta_p = J\frac{C_T}{C_P} \quad (\text{Forward}), \tag{5}$$

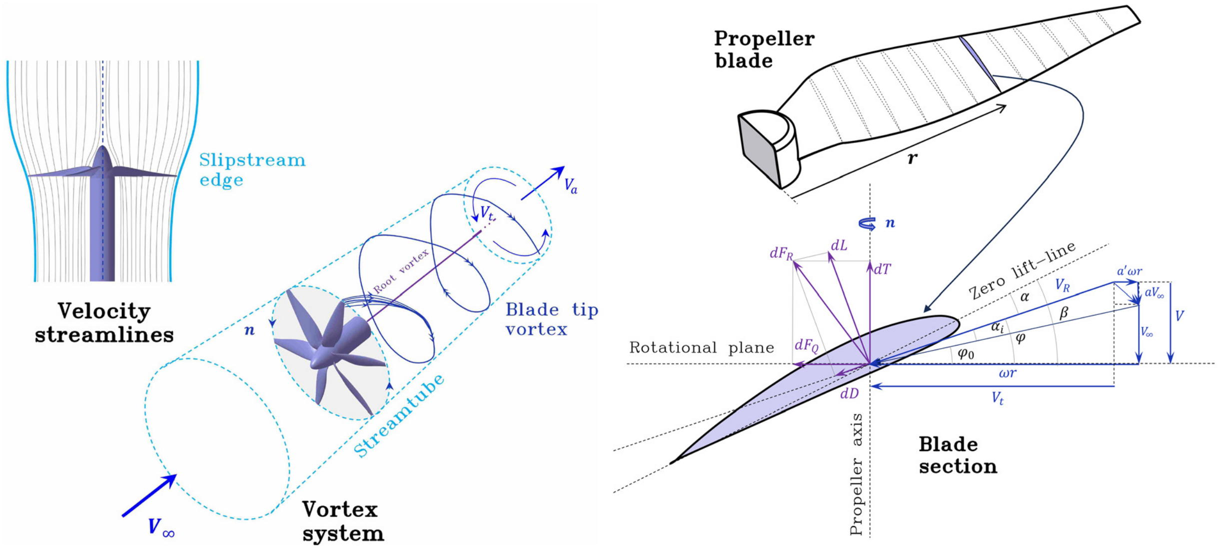

(a) Isolated propeller flow system

(b) Blade section (airfoil) velocity triangle at position r

FIG. 9. Conceptual sketch of the (a) isolated propeller flow system, showing the velocity streamlines, the streamtube, and the vortex system, and (b) blade section velocity triangle at position r.

$$FoM = \frac{C_T^{3/2}}{\sqrt{2}C_P} \quad \text{(Hover)}, \tag{6}$$

where n is the rotational speed in rev/s, ρ_∞ is the density in kg/m^3, and D_p is the diameter of the propeller in m.

In non-axial inflow conditions, such as during the transition phase of tiltrotor systems, the propeller tilt angle varies from 0° to 90°, resulting in pronounced changes in the flow structure encountered by the propeller, as well as in its aerodynamic loading and overall performance. For an isolated propeller, the freestream velocity can be decomposed into components along the propeller axis and within the rotor disk plane, giving rise to edgewise flow (see Fig. 10). This inflow orientation alters the local angle of attack experienced by each blade element and modifies the induced velocity field, and therefore the propeller aerodynamics performance.

Under this condition, the rotor blades are subjected to an asymmetric induced velocity field that varies along the azimuth. This asymmetry manifests itself between the advancing blades ($0 < \psi < \pi$) and the retreating blades ($\pi < \psi < 2\pi$) sides of the rotor disk. On the advancing side, the blades experience higher relative inflow velocities,[106,107] resulting in stronger induced flow, as described by

$$V_R = \sqrt{(V_\infty \cos \alpha_p)^2 + (\omega r + V_\infty \sin \alpha_p \sin \psi - V_{t_i})^2}. \tag{7}$$

Conversely, the retreating side encounters lower relative velocities, expressed as

$$V_R = \sqrt{(V_\infty \cos \alpha_p)^2 + (\omega r - V_\infty \sin \alpha_p \sin \psi - V_{t_i})^2}, \tag{8}$$

which is illustrated in Fig. 10. This velocity differential across the azimuth induces variation in the local angle of attack experienced by each blade section throughout its revolution, contributing to both aerodynamic imbalance and unsteady effects over the rotor disk. As reported by Ortun *et al.*,[108] dynamic of the induced velocities across the propeller disk introduces a phase lag in thrust generation, with increased thrust generation occurring in azimuthal regions where the relative inflow velocity is higher and more favorably aligned with the blade chord.

Experimental studies by Stokkermans *et al.*[35] and Zanotti *et al.*[109] found that the axial thrust increases with the tilt angle, because the blades convert the increased relative airflow into thrust more efficiently due to the higher effective angle of attack.[110] At a tilt of 90°, where the freestream is perpendicular to the propeller axis, the blades operate in edgewise flow.

Importantly, while the increase in tilt angle may enhance the instantaneous thrust, it also introduces azimuthal loading non-uniformities across the rotor disk. Moreira *et al.*[99] demonstrated that non-axial inflow produces periodic variations in the thrust, a phenomenon especially critical in low blade count propellers. The unsteady Reynolds-averaged Navier–Stokes (URANS) numerical results of Higgins *et al.*[111] reported peak-to-peak loading fluctuations of approximately 100%, relative to axial flow, under a propeller angle of 20°.

Despite favorable blade flow alignment at high tilt angles, the overall propulsive efficiency does not necessarily improve. The presence of inflow asymmetries, cross-flow components, and unsteady aerodynamic phenomena introduce additional drag and fluctuating loads. These effects increase power consumption, thereby reducing the overall propulsive efficiency. Consequently, even though thrust may increase with tilt angle, a net gain in efficiency is not guaranteed under non-axial flow or edgewise flow conditions. It is important to note that the efficiency definitions given in Eq. (5) assumes that the thrust vector is aligned with the incoming freestream velocity. This assumption breaks down when the propeller is tilted relative to the flight direction, as is common in transitional or edgewise flow regimes. To better

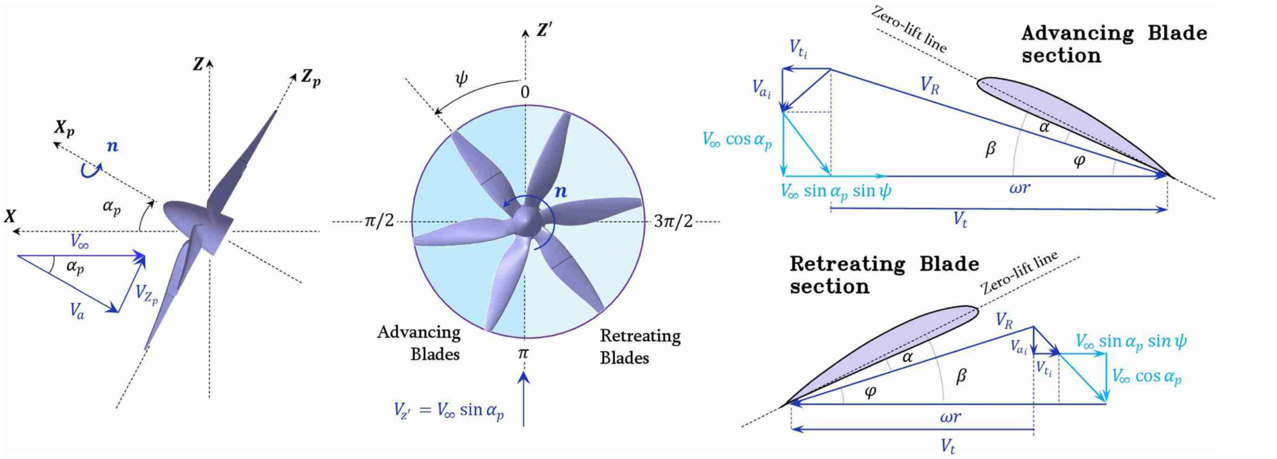

FIG. 10. Illustration of an isolated tiltrotor operating under non-axial inflow, showing velocity triangles at advancing and retreating blade sections.

capture the underlying physics under such conditions, a modified efficiency expression can be introduced by accounting for the tilt angle, α_p, and the corresponding axial component of the freestream velocity, $V_a = V_\infty \cos\alpha_p$. The corrected efficiency becomes

$$\eta_p = J\frac{C_T}{C_P}\cos\alpha_p \quad (\text{Non}-\text{axial inflow}). \tag{9}$$

Equation (9) indicates that at 90° tilt angle, the effective propulsive efficiency becomes zero, since no thrust is produced in the direction of flight. Indeed, in practical applications the propeller axis is rarely, if ever, exactly perpendicular to the freestream. For instance, in forward flight, helicopters tilt the rotor disk or tip-path plane (TPP) slightly forward by a small angle offset,[112] allowing the thrust vector to have both vertical and horizontal components. The vertical component supports the weight of the aircraft, while the horizontal component overcomes drag and provides forward motion. A similar strategy is employed by small multicopter drones, where the entire vehicle tilts forward to generate thrust in the desired direction. In contrast, for tiltrotor configurations, the 90° propeller orientation corresponds to pure hovering, not forward flight. Therefore, Eq. (9) can be considered as the general form of the propulsive efficiency, which is most appropriate for analyzing non-axial flow conditions, while classical efficiency formulations remain valid for purely axial inflow.

In this study, the analysis of isolated propeller configurations is limited to longitudinal flight, with the propeller operating in a uniform freestream flow. Under these conditions, the effective inflow angle experienced by the propeller, denoted as α_p, is defined as the angle between the freestream velocity vector and the propeller axis. Thus, whether the inclination arises from an angle of attack or a sideslip angle, the aerodynamic response of the propeller remains equivalent, as both result in the same effective inflow angle. However, in practically installed configurations, such as propellers mounted near wings or fuselage surfaces, the local flow field can be significantly altered by upwash, downwash, or crossflow effects. In such cases, the propeller may experience an effective angle of attack that differs from the freestream value. Accordingly, α_p in this study refers to the local inflow angle at the propeller disk, accounting for both freestream orientation and any local flow modifications.

The aerodynamic analysis of isolated propellers provides a necessary foundation for understanding more complex interaction phenomena, including propeller–propeller and propeller–wing effects, which are addressed in subsequent sections. These interactions are particularly critical in multirotor configurations, where they can substantially influence aerodynamic performance during the transition from hover to forward flight.

B. Propeller–propeller aerodynamics interaction

Johnson *et al.*[113] and Silva *et al.*[114] presented various eVTOL vehicle concepts that feature different propeller layouts as reference models for the development of technologies. In common with most architectures is the presence of multiple rotors working close to or downstream of each other. Therefore, these authors emphasize performance considerations arising from rotor–rotor interaction, which can significantly impact vehicle performance and noise levels, depending on the arrangement of the propellers.

The aerodynamic interaction between rotors has been extensively investigated in the literature, particularly with regard to helicopters in hover configuration.[115–117] Nevertheless, the findings of rotorcraft research may not be directly applicable to the aerodynamic interactions observed in multirotor eVTOL aircraft configurations. This difference arises from the distinctive characteristics of helicopter rotors, which typically exhibit articulated high-aspect ratio blades with relatively low twist angles. In contrast, propellers on multirotor eVTOL aircraft have smaller diameters and are designed for higher aerodynamic loading to meet the high thrust demand with compact rotor disks. Consequently, they have lower aspect ratios and larger twist angles.[34] Hence, recent research has delved extensively into the aerodynamic interactions between eVTOL propellers in various configurations.

When propellers are positioned in close proximity to each other, there is a notable impact on their performance. This proximity often leads to unsteady loading on the propeller blades and a reduction in thrust produced at a given rotational speed, typically ranging from 2% to 80%,[35,98,118–121] depending on the specific configuration and operating conditions, which leads to a decrease in efficiency. Hence, evaluating the effect of different parameters, such as longitudinal and lateral distances and propeller angle of attack, becomes crucial to analyze the effects of aerodynamic interactions on overall performance.

The conceptual representation of the propeller–propeller interaction in typical configurations, specifically one-after-another (OAA) and side-by-side (SBS) configurations, is depicted in Fig. 11. Figure 11(a) illustrates the conceptual sketch of two propellers in OAA configuration, showing the effect of the front propeller on the flow of the aft propeller. In an OAA configuration, the overlapping part of the disk experiences accelerated flow from the front propeller, which increases the total pressure difference from momentum sources such as the slipstream. The two slipstreams interfere, creating a complex flow that has attracted particular attention for a comprehensive understanding of multirotor systems and their effect on vehicle aerodynamic performance.

In Fig. 11(b), where two propellers are in side-by-side configuration, the merging of the streamtubes is less significant. However, while the inflow conditions observed in an isolated propeller are axisymmetric [see Fig. 9(a)], the presence of an adjacent propeller disrupts this symmetry. Although one might hypothesize that an infinite array of propellers would restore this symmetry, this scenario is not realistic. The conceptual representation shown here corresponds to the case where the propeller is in forward flight, with the propeller axis parallel to the incoming flow. In scenarios involving transition phase, the interactions between propellers may be more complex.

1. One-after-another configuration

In one-after-another (OAA) configuration, the slipstream of the front propeller impinges on the aft one (see Fig. 12). This interaction results in non-uniform and unsteady loading on the rear propeller disk.

Stokkermans *et al.*[35] conducted a comprehensive experimental study on different installations by varying longitudinal and lateral distances at different rotational speeds. In the OAA configuration with d_x/R_p=0.6, the thrust and power coefficients of the rear propeller start to reduce when $d_y/R_p < 2.0$, decreasing by 50% for d_y/R_p=0.5 and by 80% for d_y/R_p=0. The physical mechanism for this behavior was attributed to the combination of the induced axial and swirl velocity on the downstream propeller. The partial ingestion of the fore propeller slipstream changes the angle of attack of the aft propeller blades, depending on the combination of streamtube contraction and the composition of the blade rotation with the slipstream swirl velocity, which depends on the lateral overlap between the two propellers axis.

Zanotti and Algarotti[93] compared stereo PIV data with a vortex particle method (VPM) numerical model for one-after-another (OAA) co-rotating propellers at fixed d_x/R_p= 5 and d_y/R_p ranging from 0 to 2. Experimental flow field visualization supported by numerical solutions revealed the intricate interference between the helical structures,

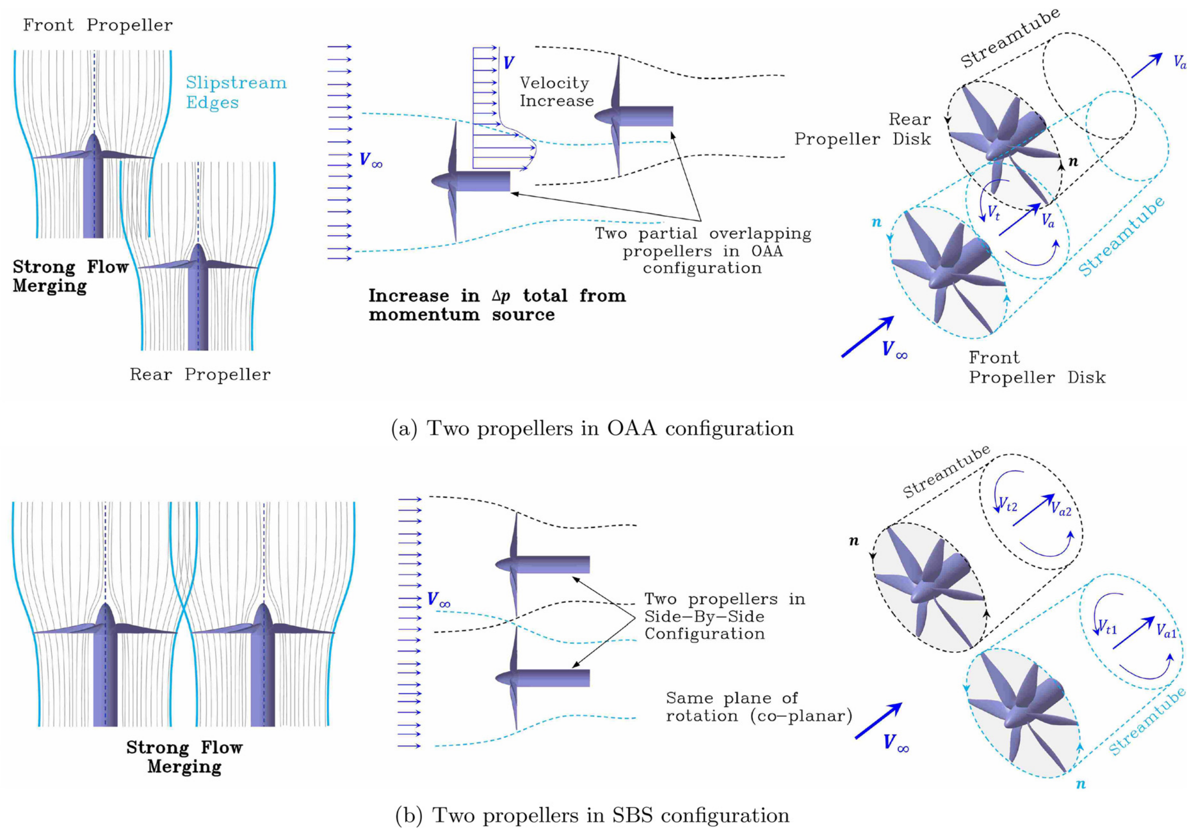

FIG. 11. Conceptual sketch of a multirotor flow system illustrating streamtube interactions: (a) two propellers in a one-after-another (OAA) configuration and (b) two propellers in a side-by-side (SBS) configuration.

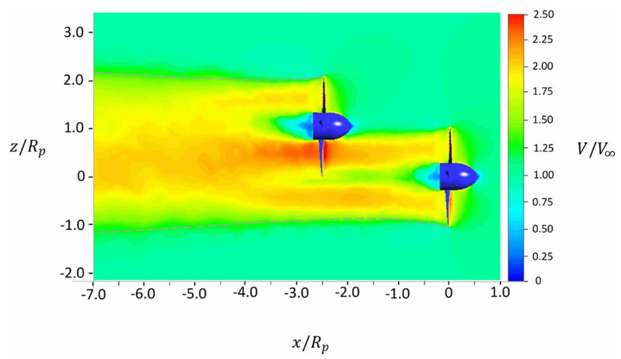

FIG. 12. Velocity magnitude contours showing the impingement of the front propeller's slipstream on the overlapping disk region of the rear propeller in OAA configuration at $J = 0.4$ and $\alpha_p = 0°$.

involving the interaction of root and tip vortices of the upstream propeller on the downstream one, depending on the lateral distance. This resulted in a 30% decrease in the thrust coefficient of the rear propeller in the coaxial installation, relative to the $d_y/R_p = 2$ configuration. Piccinini *et al.*[122] presented before a purely numerical study on the same test case based on the VPM method, where the longitudinal distance was also varied, finding a modest difference in integral performance between $d_x/R_p = 2.5$ and 6. Combey *et al.*[123] analyzed the aerodynamic interaction in one-after-another configuration for a partially overlapping propeller, and the results have shown a 12% reduction in the thrust coefficient compared to an isolated propeller. Recent GARTEUR AG-26 studies[124,125] further confirm these trends both experimentally and numerically, highlighting the performance degradation caused by closely spaced propellers.

In non-axial inflow, as discussed for the isolated propeller case in Sec. III A, the aerodynamic performance is strongly influenced by the propeller orientation, leading to more complex flow dynamics. These complexities become particularly pronounced when a propeller operates in the vicinity of another, ingesting the slipstream produced under non-axial conditions. For example, Zanotti *et al.*[109] recently provided a detailed wind tunnel analysis of two propellers in OAA configuration during transition. The study shows performance detriments that come not only from the interaction between the front and rear propellers but also from the tilting angle. These observations are consistent with the findings of Combey *et al.*,[126] who likewise demonstrated that propeller performance and interaction loads exhibit strong sensitivity to tilt angle under non-axial inflow conditions.

Figure 13 presents a summary of numerical and experimental results on the variation in the thrust coefficient of the rear propeller as a function of the lateral separation distance d_y in one-after-another configurations. Collectively, the analyzed data indicate that the thrust coefficient decreases when the lateral spacing d_y is less than the propeller diameter, regardless of the longitudinal spacing considered. Although the advance ratio also affects the trend of thrust reduction, the lateral spacing appears to be more influential in determining thrust loss, which is on the order of 30%–40% for smaller spacing ratios for co-axial propellers in most cases. The difference observed between the results of Stokkermans *et al.*[35] and Zanotti *et al.*[93] under nearly

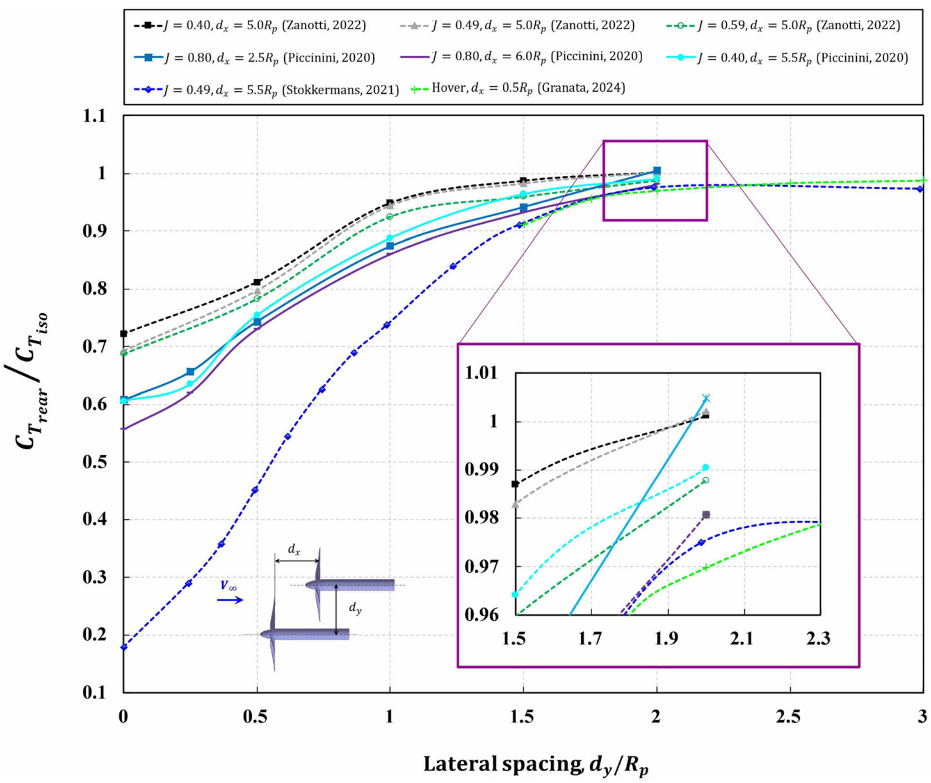

FIG. 13. Effect of lateral separation d_y on rear propeller thrust coefficient C_T in the one-after-another configuration. Dashed lines: experimental data; solid lines: numerical results. Data extracted from Refs. 35, 93, 122, and 127.

identical conditions further highlights the significant effect of propeller geometry.

2. Side-by-side configuration

For side-by-side (SBS) configuration, the rotational plane is the same for all the propellers. In forward flight with zero angle of attack of the propeller, the effect of the interaction is limited, with a loss of performance metrics generally less than 3%.[122,128]

de Vries *et al.*[94] conducted a detailed experimental campaign on three side-by-side propellers with lateral distance $d_y/R_p = 2.04$ and 3.0, also including three staggered positions. They confirmed a slight decrease in the performance of the middle propeller, up to 1.5% at maximum efficiency for the isolated case ($T_c = 0.38$), with the closest lateral arrangement. This reduction doubled for 5° incidence and was insensitive to rotation direction and blade phase angle, the latter affecting noise directivity instead. Furthermore, the study showed that the velocities induced by adjacent propeller slipstreams lead to local loading variations on the propeller disk of 5%–10% of the average disk loading. Piccinini *et al.*[122] obtained numerically similar results in terms of performance, mildly affected even at low lateral distance $d_y/R=$ 2.05, emphasizing the unsteady blade loading effects likely to improve the acoustic figures. Zanotti[34] used stereo-PIV to analyze the interaction of two unsynchronized SBS propellers with lateral distance d_y/R_p=0.2 at $J = 0.4$ and $J = 0.8$. Even if the interference effect was modest, at low advance ratio the slipstream remained less contracted than in the isolated configuration, with the wake being dragged downstream. Zhou *et al.*[98] experimentally confirmed the limited variation of the average thrust coefficient in hover, up to 2% with d_y/R_p= 2.10, accompanied by a 2.5 times higher thrust fluctuation, which the authors attributed by means of stereo-PIV visualization to the development of a separation region that is attracted toward the nearby rotor. Successive numerical studies using VPM suggested that induced upwash was the main cause of blade loading reduction, with a negligible effect of the recirculation region.[119] Shukla and Komerath[129] employed high-speed stereo PIV focusing on different rotor separations and Reynolds numbers. They observed a stronger wake interaction at lower Reynolds (40 000), arguing that the larger tip vortex size increased the induced velocity and unsteady loading for closely spaced rotors ($d_y/R_p = 2.1$). Veismann *et al.*[130] measured in the wind tunnel the performance of paired counter-rotating small-scale rotors during axial descent, using three rotor sizes. The authors found that for $d_y/R_p > 3.0$ the rotor characteristic is close to that in isolation. For smaller spacings, increased peak fluctuations were observed and found to correlate with mean thrust losses, also depending on the blade geometry. Chae *et al.*[131] carried out experimental tests of small tandem rotors in crosswind at varying wind velocities and rotor separations. The thrust coefficient of the downstream rotor was measured to decrease for smaller separations and at a faster rate with increasing crosswind velocity, up to 5% compared to an isolated case, with $d_y/R_p = 2.25$. The authors analyzed the mechanisms of thrust reduction using stereo-PIV data, attributed to the higher induced axial velocities on the rotor, which were concentrated on the centerline and retreating side at low crosswind speeds but extended to the advancing side at greater speeds.

In addition to experimental studies, several authors used numerical frameworks to investigate the propeller–propeller interaction in different configurations. Ko *et al.*[132] used a free-wake vortex-lattice method (VLM) to investigate the wake interaction of a quadcopter at varying forward flight speed, incidence angle, and advance ratio for a cross-type or plus-type orientation of the four rotors. The study measured the change in thrust coefficient between the different rotors, showing a non-monotonic variation that was qualitatively similar to an isolated rotor, with differences based on the position and orientation of the rotor, and interpreting the results using the induced velocity concept. Misiorowski *et al.*[133] run detached eddy simulations (DES) on a vehicle of the same type, finding that with the plus configuration in forward flight, the propeller–propeller interaction is less severe and the lateral propellers can generate more lift due to the upwash induced by the front propeller. Barcelos *et al.*[134] used a potential flow method corrected for viscous effects. Their results compare well with those of Misiorowski[133] and indicate that the aerodynamic interference increases at higher angle of attack and lower advance ratio, with the plus configuration reaching up to 3.5% higher efficiency than the square configuration. Pinti *et al.*[135] built a multi-fidelity surrogate of data collected with different propeller spacings in a multicopter in forward flights, with two propellers aligned longitudinally. The authors used a CFD solver in conjunction with a lower fidelity BEM with wake model and estimated a prominent impact of the longitudinal distance on the thrust coefficient of the aft propeller, with an overall variation of around 8% from $d_x/R_p = 4$ to $d_x/R_p = 2.5$. Healy *et al.*[136] employed DES for a similar case, investigating the effect of canting the propeller axis. The authors observed that regardless of cant orientation, the wake of the front propeller induces downwash on the aft one, creating a lift deficit. The aft propeller canting direction, with the advancing side up or down and longitudinally, has different effects on the force vector orientation and the nose-down and roll pitching moments. For example, uncanted/laterally canted aft propellers experience moderate thrust penalties (15%–18%) and pitching moment changes (55%–64%), while longitudinal canting can reduce lift from 10% to 20% and strongly vary the nose-down pitching moment. Qiao *et al.*[97] carried out a study on propeller installation for distributed propulsors using CFD with different propeller fidelities. Using unsteady RANS simulations, the authors optimized an over-the-wing installation with three propellers, obtaining a 14.2% higher efficiency due to favorable interference.

The summary of selected results on the performance of side-by-side propellers is illustrated in Fig. 14. The performance decrease compared to an isolated propeller in hover and forward flight is shown to be relatively small, with differences of less than 3%. For horizontal flight, where the propeller axes are parallel to the freestream velocity, the interactions do not significantly affect the performance of adjacent propellers, as they are all in the same plane (co-planar) and do not operate within the wake or slipstream of another propeller. However, any downstream elements, such as lifting surfaces, may experience a strongly non-uniform and disturbed flow field. However, when the propeller axes are perpendicular to the incoming flow, as studied by Stokkermans,[35] the propellers operate in an edgewise flow, and the performance of the rear propeller compared to an isolated propeller can exhibit significant reductions, with differences reaching up to 30%.

All findings in this section indicate that the performance of side-by-side propellers is minimally affected, with observable influences appearing only at very low separation distances. No significant aerodynamic drawbacks have been identified for such configurations. However, the differences in flow characteristics for different operating

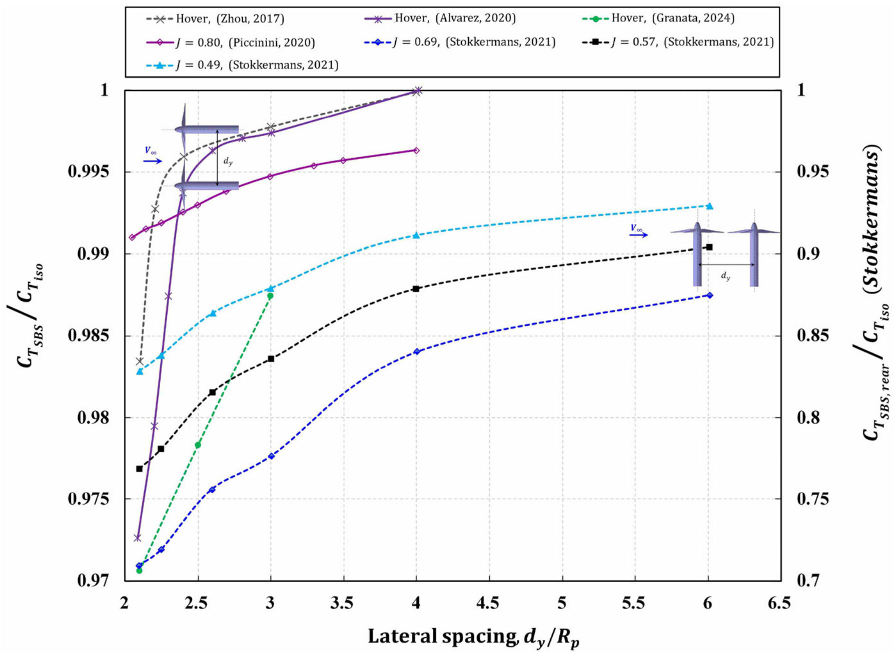

FIG. 14. Effect of lateral separation d_y on thrust coefficient C_T of the side-by-side (SBS) configuration. Dashed lines: experimental data; solid lines: numerical results. Data extracted from Refs. 35, 98, 119, and 122.

conditions suggest potentially higher aerodynamic and aeroacoustic effects through a typical eVTOL flight mission, which warrant further investigation to ensure optimal performance.

C. Propeller–wing aerodynamics interaction

In addition to propeller–propeller interactions, the aerodynamic coupling between propellers and lifting surfaces is a critical consideration in the integrated design of eVTOL aircraft. In many UAM configurations—particularly wing-mounted distributed electric propulsion (DEP) systems such as the Airbus Vahana A^3[59] and Joby S4,[61] propellers are positioned in close proximity to the wing, either upstream, downstream, or above it. These installation effects give rise to complex flow phenomena that influence both the propeller and the wing, often resulting in significant deviations from isolated component behavior.

When a propeller operates near a wing, the local flow field is shaped by mutual aerodynamic interaction: the presence of the wing alters the inflow conditions experienced by the propeller blades, modifying loading distribution and inducing unsteady aerodynamic effects; conversely, the propeller slipstream modifies the wing's pressure field, thereby affecting lift, drag, and stall behavior.[137–139] As illustrated in Fig. 15, the propeller slipstream impinging on the wing surface modifies the local circulation, thereby altering the spanwise lift distribution. This induces localized up-wash and down-wash, depending on the propeller rotation direction (inboard-up or outboard-up). These interactions can either enhance or degrade overall aerodynamic performance, depending on the relative position of the propeller to the wing, its rotation direction, inflow angle, flight regime, and the geometry of both the propeller and the lifting surface.

As these phenomena are particularly critical for UAM designs employing multiple propellers distributed along lifting surfaces (see Fig. 16), a detailed understanding of propeller–wing aerodynamic interactions is essential to achieving optimal aerodynamic efficiency and flight control. Accordingly, this section examines the aerodynamic characteristics of propeller–wing integration, with emphasis on the mutual influence between the wing and the propellers, and the resulting effects on lift-to-drag ratio (L/D), spanwise lift distribution, and propeller performance.

Depending on the relative positioning of the propeller with respect to the wing, several configurations can be identified: tractor, pusher, over-the-wing (OTW), and under-the-wing (UTW), as illustrated in Fig. 17. When the lateral position of the propeller coincides with the wingtip, i.e., $L_y = b/2$, the configuration is referred to as wingtip-mounted. Additionally, when the propeller is embedded within the wing, it may be classified as an in-wing embedded configuration.

These configurations generate distinct interaction phenomena between the propeller and wing that influence aerodynamic performance across various flight phases. In tractor configurations, a key mechanism involves the propeller slipstream impinging on the wing's leading edge, modifying local pressure distribution and boundary-layer behavior.

Gao *et al.*[140] demonstrated that DEP tractor setups induce upwash and downwash effects depending on the direction of propeller rotation, increasing lift by up to 34% compared to a clean wing (see Table IV). Beckers *et al.*[141] and Keller[142] reported lift enhancements of up to 63% and 42%, respectively, attributed to increased dynamic pressure and delayed flow separation within the propeller slipstream. Xue and Zhou[143] observed lift-to-drag ratio improvements up to 51%, while Aref[107] showed that inboard-up rotation yields higher lift than outboard-up due to more favorable swirl interactions. The slipstream decreases the pressure on the upper surface of the wing and increases it on the lower surface, with the local swirl governing the intensity of these effects. In upwash regions, swirl contributes to higher dynamic pressure, while in downwash regions it can have an opposing,

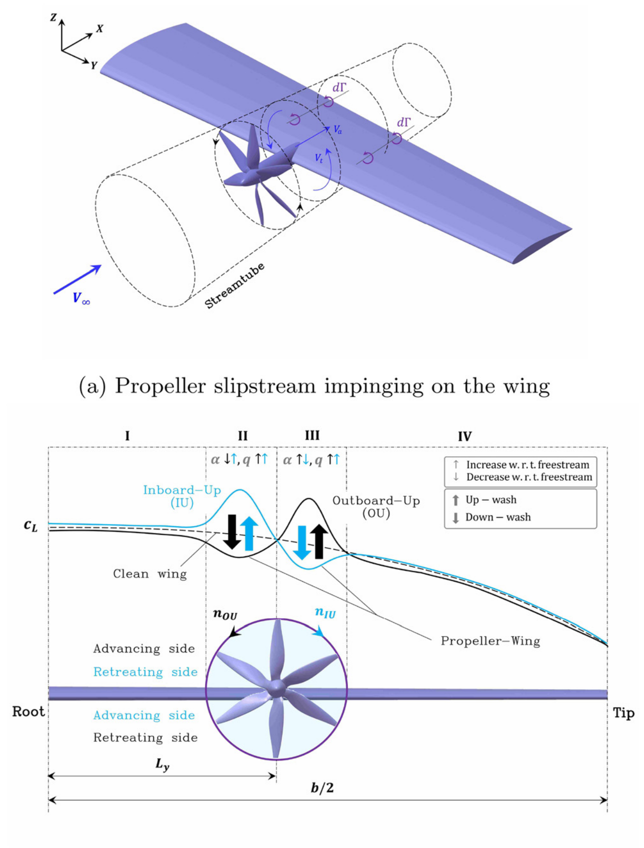

(a) Propeller slipstream impinging on the wing

(b) Spanwise lift distribution distortion

FIG. 15. Conceptual sketch of propeller–wing flow system, showing the effect of the propeller induced axial (V_a) and tangential velocity (V_t) on the on spanwise lift coefficient (c_L) distribution of the wing.

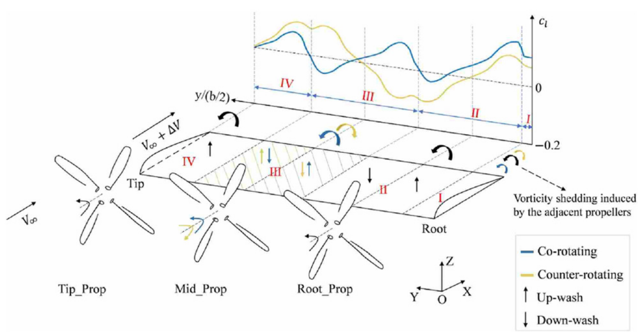

FIG. 16. Schematic of multirotor–wing aerodynamic interactions. Reproduced with permission from Gao *et al.*[140] Copyright Copyright 2025 Elsevier Masson SAS. All rights reserved.

pressure-reducing influence.[144] Seo *et al.*[145] highlighted a trade-off: while increasing the number of propellers improves the lift-to-power ratio, it may reduce both the lift-to-drag and thrust-to-power ratios, depending on configuration. Despite these aerodynamic benefits, adverse effects also emerge. The high-velocity slipstream accelerates boundary-layer transition, increasing skin friction and unsteady aerodynamic behavior.[146] Zawodny *et al.*,[147] through experimental and numerical analyses, observed that close propeller–wing spacing leads to mutual interference. The wing's potential field distorts the upstream inflow into the propeller, while the propeller wake intensifies suction peaks near the wing's leading edge. Additionally, unsteady tip vortex impingement was shown to cause impulsive loading at the wing leading edge, with potential implications for structural fatigue and acoustic emissions.

In pusher configurations, the propeller is positioned downstream of the wing, ingesting its wake. This setup results in fundamentally different interaction mechanisms compared to the tractor case. Rather than modifying the upstream flow, the wing alters the propeller's inflow by introducing non-uniformities caused by its wake, boundary layer, and trailing-edge vortices. Lei *et al.*[148] demonstrated through experiments and simulations that the pusher propeller has negligible influence on wing lift at angles of attack below 16°. Beyond this value, this configuration can enhance lift by 73%–87% without degrading the L/D ratio, although the drag coefficient was found to be higher than that of the isolated wing. Serrano *et al.*[149] showed that placing the propeller hub closer to the wing's trailing edge improves propeller efficiency by ingesting lower velocity wake flow. Elevating the propeller vertically was also found to increase wing lift while reducing parasitic drag. In this configuration, the wing wake and trailing-edge vortices induce non-uniform inflow and unsteady loading on the propeller blades. These fluctuations can lead to increased noise levels, an effect discussed further in Sec. IV C.

In over-the-wing (OTW) configurations, the propeller is mounted above the wing, accelerating the flow over the upper surface without direct impingement or flow ingestion. This acceleration lowers the local static pressure and thereby enhances lift. Reynard *et al.*[150] conducted comprehensive wind tunnel experiments to investigate propeller–wing interactions in OTW configuration. Their results showed that the propeller induces an adverse pressure gradient on the wing. Increasing blade-tip clearance was found to reduce thrust due to slipstream contraction and flow deceleration near the wing surface. Although tip clearance affected surface pressure fluctuations and increased time-averaged pressure, it did not effectively prevent flow separation. Notably, even when blade tips were located outside the boundary layer ($\varepsilon = 3\delta_{99}$), separation persisted. This was attributed to the slipstream forming a high-momentum boundary that created a divergent flow channel between the slipstream edge and the flap surface, intensifying the adverse pressure gradient and triggering separation. The study concluded that, under the tested conditions, the dominant mechanism for flow separation was the adverse pressure gradient rather than periodic excitation from tip vortices. Further support for the lift-enhancing potential of OTW configurations was provided by Qiao *et al.*,[97] who performed a numerical analysis comparing OTW and tractor configurations. Their results, summarized in Table V, show improved aerodynamic performance in the OTW case, including increased L/D ratio. Flow visualizations presented in Fig. 18 highlight the merging and acceleration of flow over the wing in the OTW setup, explaining the performance improvement.

Wingtip-mounted propellers offer aerodynamic advantages by reducing induced drag and recovering energy from wingtip vortices. By positioning the propeller near the wingtip, the induced swirl

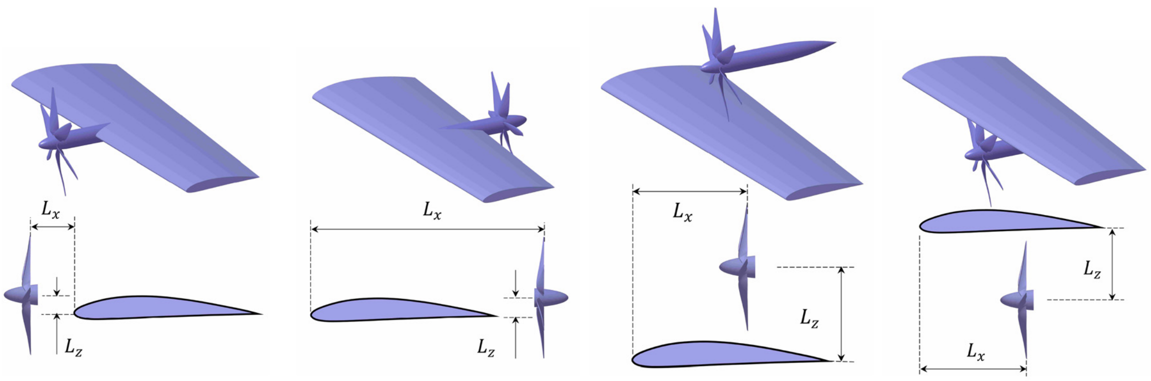

FIG. 17. Typical propeller–wing configurations.

TABLE IV. Comparison of time-averaged lift coefficient at $J = 0.85$, $\alpha = 4^\circ$ for three tractor propellers configurations.[140]

Case	C_L	ΔC_L (%)
Clean wing	0.2805	...
Co-rotating	0.3768	34.33
Counter-rotating	0.3304	17.79

interacts with the natural tip vortex, weakening its strength and converting otherwise wasted rotational energy into useful thrust.

Sinnige *et al.*[151] experimentally demonstrated that wingtip-mounted propellers with inboard-up rotation can reduce induced drag by up to 15% while maintaining or even enhancing the overall lift generated by the wing. Their study highlighted the critical role of propeller rotation direction in modifying the tip vortex behavior. In particular, outboard-up rotation was shown to reinforce the wingtip vortex, causing downwash inflow to the wing, thereby increasing induced drag and reducing the lift coefficient (C_L).

As shown in Table VI, the aerodynamic response of the wing-propeller system exhibits a strong dependency on both rotation direction and operating point. For the inboard-up configuration, C_L increases significantly with decreasing advance ratio J, reaching a maximum increase in 56.25% at $J = 0.7$ relative to the propeller-off case. In contrast, the outboard-up configuration exhibits the opposite trend: C_L decreases with increasing thrust, resulting in a 22.22% reduction at $J = 0.7$ compared to the propeller-off baseline. These findings underscore the sensitivity of lift generation to rotation-induced vortex interactions in wingtip-mounted propulsion systems.

TABLE V. Performance comparison of tractor and OTW configurations. Data from Ref. 97.

	Single-propeller (RPM = 4800)			Two propellers (RPM = 3900)		
Performance	Tractor	OTW	Δ(%)	Tractor	OTW	Δ(%)
Lift (N)	582	590	+1.3	1140	1149	+0.7
L/D (–)	15.2	60.0	+294	15.74	30.20	+92
Thrust (N)	257	238	−7.4	308	273	−11.3
Power (kW)	12.6	12.5	−0.8	13.3	12.8	−3.8
Froude η_p (–)	0.56	0.52	−6.4	0.64	0.59	−7.8
Overall η_p (–)	0.476	0.502	+5.5	0.487	0.505	+3.8

Numerical investigations by Minervino *et al.*[152] predicted drag reductions of 6%–10% during cruise and climb phases, along with notable alterations in the spanwise lift distribution. While local skin friction drag may increase within the propeller slipstream, the overall induced drag is generally reduced. Recent experimental work by Zanotti *et al.*[153] further confirmed improvements in lift and propeller efficiency at high advance ratios, especially for short-boom configurations. However, unsteady aerodynamic effects, such as flow fluctuations and pressure oscillations, commonly observed in tractor and pusher arrangements, are also present in wingtip-mounted configurations and must be carefully addressed during the design process.

In under-the-wing (UTW) configurations, the propeller is mounted below the wing, accelerating airflow over the lower surface and directly interacting with the boundary layer. While this setup can provide aerodynamic benefits, it introduces structural challenges, most notably the need for increased ground clearance, which may necessitate taller landing gear, leading to added weight and drag. As a result, UTW arrangements have received relatively little attention in urban air mobility (UAM) vehicle design. However, foundational studies by NASA, such as the Quiet Clean Short-Haul Experimental Engine (QCSEE) program,[154] demonstrated that nacelle blowing in UTW configurations can suppress flow separation on the lower wing surface and reduce installation drag.

In the in-wing embedded configuration such as Ascendance Flight Technologies,[155] the propeller is integrated within the wing structure, re-energizing the boundary layer and potentially delaying separation, thus lowering form drag. Despite these advantages, few studies have explored this setup in depth. Recent investigations into embedded propulsion concepts,[156–158] reported favorable lift-to-drag ratios (L/D up to 12.7 at 4° angle of attack), indicating promising aerodynamic performance. Nonetheless, research remains limited,

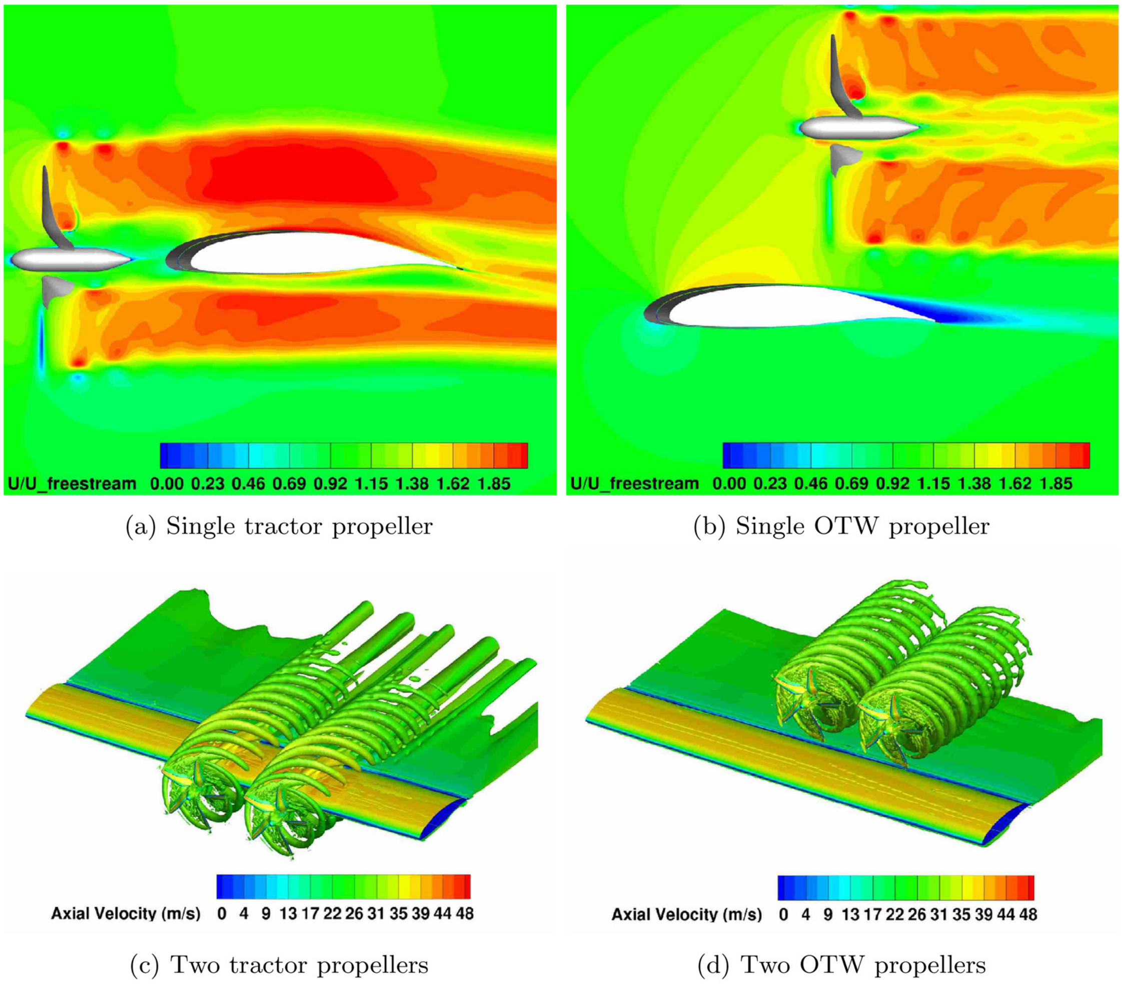

FIG. 18. Flow visualization of the tractor and over-the-wing (OTW) configurations: (a) and (b) instantaneous axial velocity and (c) and (d) iso-surfaces of Q-criteria at a value of 0.01, colored using axial velocity. Reproduced from Ref. 97, licensed under a Creative Commons Attribution (CC BY) license.

TABLE VI. Effect of propeller rotation direction and advance ratio on the wingtip-mounted configuration at $\alpha = -0.2^\circ$ (inboard-up) and $\alpha = +0.2^\circ$ (outboard-up). Data from Ref. 151.

Operating point		C_L	
J	C_T	Inboard-up	Outboard-up
Prop-off	⋯	0.16	0.18
1.0	0.014	0.16	0.18
0.9	0.053	0.18	0.17
0.8	0.095	0.21	0.16
0.7	0.123	0.25	0.14

particularly regarding full-scale applications in distributed electric propulsion systems.

Table VII presents a summary of the aerodynamic characteristics associated with various propeller–wing configurations, based on the reviewed literature and the work of de Vries *et al.*[159] In the table, a "+" symbol denotes an increase in a given parameter, while a "–" indicates a decrease. Red coloring is used to highlight detrimental effects, whereas green indicates beneficial effects. In cases where the effect of a configuration on a parameter depends on factors such as propeller position or operating conditions, the symbol "/" is used to denote a variable or mixed influence.

Both experimental and computational studies consistently show that propeller–wing interaction significantly influences aerodynamic performance. These effects are highly sensitive to factors such as propeller placement, wing geometry, rotation direction, inflow conditions, and the number of propellers. Careful consideration of these parameters is crucial for enhancing lift, delaying stall, and improving overall efficiency in UAM aircraft. However, these interactions also introduce unsteady aerodynamic loads that may cause pressure fluctuations on the wing and propeller surfaces, contributing to increased noise, a topic explored in the following section.

TABLE VII. Summary of propeller–wing configurations and their performance characteristics. Rating: + = increase, − = decrease, Green = beneficial, red = not beneficial.

Configuration	Propeller relative position	Effects on propeller–wing system			
Tractor	Upstream of wing, accelerates flow over wing	Strong impact on lift	+ + +	Moderate impact on η_p	++
		Moderate impact on drag	−− / ++	Moderate impact on noise	++
Pusher	Downstream of wing, ingests wing wake	Minor impact on lift	+	Moderate impact on η_p	++
		Minor impact on drag	+	Strong impact on noise	+ + +
OTW	Above wing, accelerates flow over wing upper surface	Moderate impact on lift	++	Strong impact on η_p	− − − / +
		Strong impact on drag	− − − / +	Strong impact on noise	+ + + /−
UTW	Below wing, accelerates flow over wing lower surface	NA		NA	
		NA		NA	
Wingtip-mounted	At wingtip, affects tip vortex system	Moderate impact on lift	++/−−	Moderate impact on η_p	++
		Strong impact on drag	− − −	Moderate impact on noise	+ /−−
In-wing embedded	Within the wing volume, ingests boundary layer	NA		NA	
		NA		NA	

IV. MULTIROTOR AEROACOUSTICS

A. Single propeller aeroacoustics

From the standpoint of social community acceptance, it is essential to understand the nature of propeller noise, such as its sources and constitutional components during operation. This section focuses on the noise characteristics of a single, isolated propeller, addressing the aforementioned aspects without accounting for installation effects such as propeller–wing or propeller–propeller interactions. However, it is important to recognize that installation effect represents the key distinction between laboratory environment and real-world scenarios and their impact on the noise emission of multirotor vehicle should not be underestimated. These effects are discussed in detail in other sections, while the current section aims to provide a comprehensive understanding of the fundamental noise-generating mechanisms associated with a single propeller.

Based on the frequency-domain characteristics, propeller noise mainly consists of harmonic (tonal) and broadband components. The former is periodic in nature,[160] with a fundamental frequency f as a function of the number of blades B and rotational speed n, i.e., $f = B\,n$. Since the resulting pressure waveform is rarely sinusoidal, this noise occurs at multiple harmonics at the integer multiples of f. This can be understood by expressing the periodic noise signal in a Fourier series expansion, which the noise signal is decomposed into a sum of sinusoidal components at the fundamental frequency and its harmonics. The harmonics noise is directly due to the sound pressure waves generated by the relative motion between the rotating blades or their induced flow and the surrounding medium.[161] They generally appear more pronounced at low frequencies, and originate from both steady and unsteady aerodynamic loading, as well as the periodic displacement of air by the rotating blades. The former can be attributed to the thrust and torque acting on the blades (rotational noise[162]), and the latter is associated with the interactions with the wake shed by preceding blades [blade–vortex interaction (BVI)].[160]

Broadband noise is another significant component of propeller noise, characterized by its energy being distributed over a range of frequencies due to the involvement of various flow phenomena spanning different temporal and spatial scales. This type of noise arises from several mechanisms, including turbulence in the inflow impinging on the blades, turbulent boundary layer passing the blade trailing edge, and the formation and shedding of tip vortices.[160,163,164] Broadband noise is typically the dominant contributor to propeller noise at high frequencies;[163,165] however, it is generally less irritating compared to harmonic noise when evaluated using perceived noise level metrics.[161] High-frequency broadband noise also experiences more significant attenuation over long distances due to molecular absorption effects,[164] which disproportionately affect sound waves with short wavelengths (i.e., high wavenumbers).

Propeller noise under non-axial inflow conditions ($\alpha_p \neq 0°$), commonly encountered during transition phases of tiltrotor configurations, differs significantly from the axial case ($\alpha_p = 0°$). The periodic variations in local angle of attack across the propeller disk induce fluctuating forces that alter tonal noise generation mechanisms.

Romani *et al.*[166] conducted a high-fidelity aeroacoustic analysis of a two-bladed, low-speed propeller (tip Mach number $M_{\text{tip}} = 0.23$) at a 15° tilt using lattice-Boltzmann very large eddy simulation (LBM-VLES) coupled with the Ffowcs Williams–Hawkings (FW–H) acoustic analogy. Their results showed a substantial increase in tonal noise: sound pressure level (SPL) at the first blade passing frequency (BPF1) rose by up to 6 dB on the advancing side of the disk, while sound power level (PWL) increased by 3.4 and 2.1 dB at BPF1 and BPF2, respectively. In the 1/12-octave band, SPL increased by as much as 8 dB at BPF1. These effects were attributed to tilt-induced unsteady loading, which dominated tonal radiation. Conversely, broadband noise showed minimal sensitivity to inflow angle. Building on this work, Yunus *et al.*[167] employed and validated two low-fidelity prediction tools, LOPNOR and Opty ∂ B, that extend classical Blade Element Momentum Theory (BEMT) by incorporating azimuthal variations in blade incidence. Using the same 15° inflow condition, both models reproduced thrust, torque, and far-field sound pressure levels (SPL) with acceptable agreement relative to LBM-VLES simulations and experimental data, for a fast prediction. These tools offer a computationally efficient means for predicting tonal noise, capturing similar amplification trends, particularly at BPF1 and BPF2.

These findings underscore that unsteady aerodynamic loading, induced by propeller tilt, is the dominant mechanism driving tonal noise in low-speed, isolated propellers, while broadband contributions remain largely unaffected. However, both studies were limited to a single tilt angle (15°), emphasizing the need for a broader parametric study across the transition regime. Such insights are critical for multirotor systems, where complex propeller–propeller interactions under non-axial, unsteady inflow can further amplify noise. A solid understanding of isolated propeller behavior is therefore a prerequisite to accurately assess multirotor aeroacoustic coupling.

B. Propeller–propeller aeroacoustics interaction

Noise generated by a single propeller can be significant, but it is often further intensified in multirotor systems due to aerodynamic interactions between adjacent propellers. Figure 19 illustrates potential multirotor interaction noise sources in UAM vehicles. For closely spaced propellers, mutual wake impingement and intensified tip–vortex interactions increase unsteady aerodynamic loading, which primarily enhances tonal radiation through blade–vortex and blade–wake mechanisms. In parallel, broadband noise becomes a significant contributor to the overall acoustic signature. It mainly originates from the turbulent boundary-layer interaction with the trailing edge, which is generally regarded as the dominant mechanism in propeller broadband emission. Increased inflow turbulence, caused by propeller–wake interactions, enhances the unsteady boundary-layer fluctuations, modifying the spectral content and amplifying the broadband radiation.[168] Studies indicate a thrust penalty and a substantial increase in thrust fluctuations, along with a significant noise increase as propeller spacing decreases.[98,119,169] Additionally, propeller–propeller interactions strongly influence the noise directivity pattern,[170–172] which can be actively controlled through adjustments of relative blade phase angles, analogous to synchro-phasing in turboprop airplanes.[173–175] However, such local noise mitigation requires precise monitoring of rotational speeds and phase angles, which remains challenging in practice.[176] Additionally, broadband emissions cannot be easily mitigated through phase-control strategies that primarily target tonal noise, although such strategies have been reported to modulate their amplitude.[177,178]

1. One-after-another configuration

A primary concern in one-after-another (OAA) propeller configurations is the unsteady aerodynamic loading experienced by the downstream propeller due to the non-uniform inflow generated by the wake of the upstream propeller. This inflow typically contains vortical structures and axial velocity gradients, resulting in periodic variations in blade loading. These unsteady interactions increase acoustic emissions, notably in the form of both tonal and broadband noise.

Recent experimental and numerical studies have emphasized the critical role of propeller spacing, both axial (d_x) and lateral (d_y) in shaping the aeroacoustic signature of OAA systems. Paruchuri *et al.*[179] investigated the influence of these spacings on the far-field noise generated by OAA propellers. The study revealed a pronounced sensitivity of the overall sound pressure level (OASPL) to lateral separation. For lateral distances greater than twice the propeller radius ($d_y > 2R_p$), the OASPL consistently remained below 73 dB across all axial separations. In contrast, configurations with complete disk overlap exhibited significantly higher noise levels, exceeding 85 dB, thus highlighting the detrimental acoustic effects of overlapping propeller disks.

Bu *et al.*[180] experimentally measured the acoustic behavior of OAA propellers under various spatial configurations. Their findings

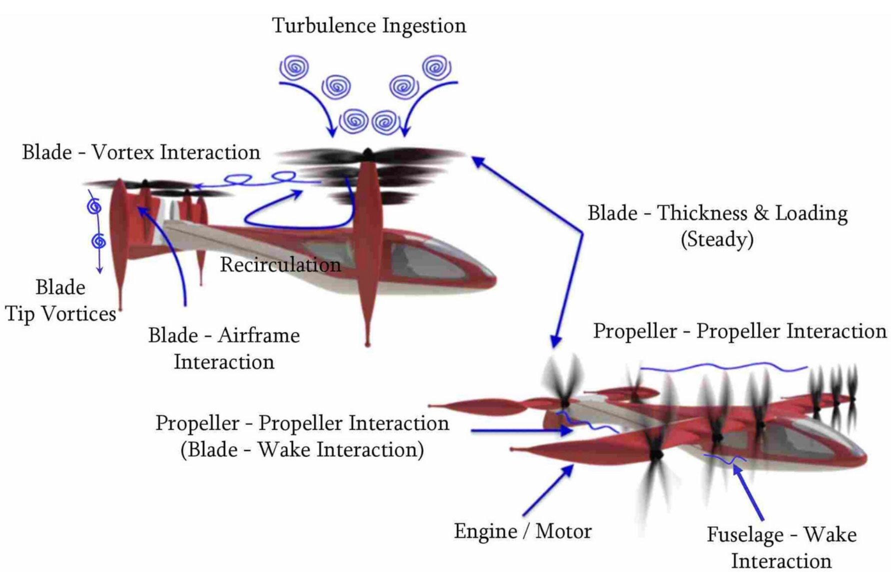

FIG. 19. Potential multirotor noise sources on UAM vehicle. Adapted from Ref. 89.

showed that tonal noise levels increased by up to 10 dB at lower observation angles when the propellers were in close proximity. Meanwhile, broadband noise exhibited smaller variations, typically within 3 dB.

Granata *et al.*[127] conducted a coupled aerodynamic and aeroacoustic experimental campaign to quantify the noise penalties associated with partial disk overlap in OAA configurations. The measurements revealed that such overlap induced increased noise levels due to the high amplitude of periodic fluctuations in the aerodynamic loading of the downstream propeller. By varying both lateral (d_y) and axial (d_x) spacings, the study identified how the spacing affects the aerodynamic loading and the resulting aeroacoustic emissions. At a fixed longitudinal separation of $d_x = 0.5R_p$, a reduction in lateral spacing from $d_y = 2.5R_p$ to $d_y = 2R_p$ led to a modest decrease in noise, attributed to diminished wake interaction. However, further reduction to $d_y = 1.5R_p$ resulted in a noise increase in up to 4 dB in the forward direction. Additionally, counter-rotating configurations exhibited slightly higher sound pressure levels than co-rotating ones, in line with the greater aerodynamic interaction previously observed by Caccia *et al.*[181] More recently, Turhan *et al.*[182] provided additional evidence that lateral spacing plays a significant role in the acoustic radiation of OAA systems. For a lateral offset corresponding to 40% of the propeller diameter, tonal noise levels increased by up to 18 dB relative to non-overlapping configurations, a rise attributed to stronger blade–vortex and blade–wake interaction mechanisms.

Taken together, these results underscore the strong sensitivity of the aeroacoustic performance of OAA configurations to both lateral and axial propeller spacing. As illustrated in Fig. 20, for microphone positions located at a distance of $12R_p$ from the origin [refer to Fig. 20(a)], reduced lateral spacing leads to high increases in radiated noise. Specifically, as shown in Fig. 20(b), a lateral spacing of $d_y = 1.5R_p$ yields an increase in up to 5 dB at an angle of 30° compared to the $d_y = 2.5R_p$ case. Likewise, variations in axial spacing, as presented in Fig. 20(c), exhibit a comparable influence on sound pressure levels. For the configuration considered, reductions in axial spacing can result in noise increases of up to 3.34 dB at 30° for $d_y = 1.5R_p$ relative to $d_y = 2.5R_p$. In addition to geometric parameters, the operational condition, particularly the advance ratio, also has a notable impact on tonal noise characteristics. As shown in Fig. 21, higher advance ratios (e.g., $J = 0.66$) are associated with reduced overall sound pressure level (OASPL) in comparison to lower advance ratios (e.g., $J = 0.33$).

Despite recent progress, the aeroacoustic behavior of OAA multirotor configurations remains insufficiently characterized. While most existing studies have focused on two-propeller arrangements with planar spacing in the x and y directions (d_x, d_y), practical eVTOL architectures often incorporate more than two propellers and introduce vertical spacing in the z direction (d_z). This added spatial complexity necessitates a more comprehensive aeroacoustic analysis to accurately capture the influence of three-dimensional propeller placement on radiated noise. In addition, the transition phase of flight presents a particularly challenging regime due to rapidly varying inflow angles, unsteady blade loading, and complex wake interactions, all of which can introduce additional tonal and broadband noise components. Furthermore, the role of blade phase synchronization, specifically whether propellers operate in-phase or out-of-phase, remains largely underexplored, despite its known influence on tonal noise characteristics and spectral directivity.

2. Side-by-side configuration

In side-by-side (SBS) multirotor configurations, significant aeroacoustic challenges arise from propeller–propeller interactions that become more pronounced as lateral spacing decreases. The lateral center-to-center distance between adjacent propellers, denoted in this work as $d_y = 2R_p + s$, where R_p is the propeller radius and s is the tip-to-tip blade clearance, plays a critical role in determining the intensity of the noise.

Zhou *et al.*[98] demonstrated that, in an SBS configuration, as d_y decreased, both thrust fluctuations and sound pressure levels increased. The variation in sound pressure level (SPL) is shown in Fig. 22. At a reduced spacing of $d_y = 2.1R_p$, the measured SPL increased by

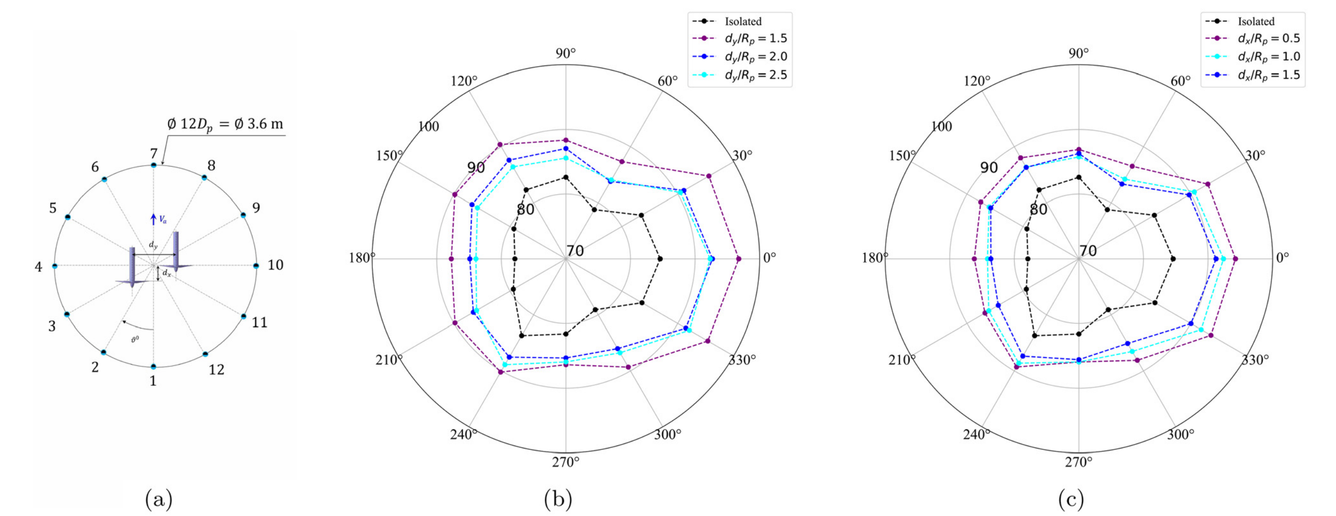

FIG. 20. Directivity of overall averaged SPL for the one-after-another (OAA) co-rotating propeller configuration in hover ($V_\infty = 0$): (a) microphone positions; (b) effects of lateral spacing at fixed axial spacing $d_x = 0.5R_p$; and (c) effects of axial spacing at fixed lateral spacing $d_y = 2.5R_p$. Data extracted from Ref. 127.

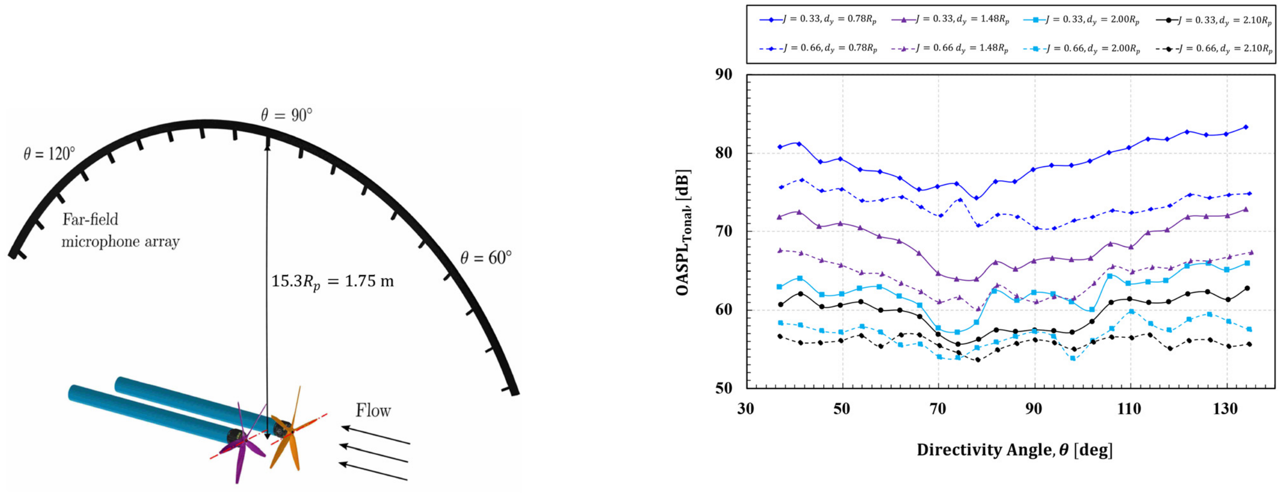

(a) Microphone positions (b) $OASPL_{Tonal}$

FIG. 21. Effect of lateral spacing on tonal overall sound pressure level (OASPL) directivity for the OAA propeller configuration at advance ratios $J = 0.33$ and $J = 0.66$. (a) Reproduced and (b) data extracted from Ref. 182, licensed under a Creative Commons Attribution (CC BY) license.

approximately 3 dB compared to $d_y = 4R_p$ at a location directly upstream of the propellers. Their spectral analysis revealed an increased tonal component at the blade-passing frequency (BPF) and its harmonics, with broadband noise also rising due to the increased turbulence kinetic energy (TKE) and loading fluctuations. The unsteady pressure fields generated by tip vortex and blade–wake interactions between adjacent rotors were identified as the dominant contributors to the observed acoustic degradation. Similarly, Alvarez *et al.*[96] examined aeroacoustics interactions between adjacent rotors in a multirotor system using URANS and VPM methods. They found that reducing tip-to-tip distance increases noise up to 10 dBA beneath the rotors, while downstream spacing of half a diameter reduces noise by 4 dBA without affecting aerodynamic performance.

Jia and Lee[183] conducted high-fidelity numerical simulations of SBS rotor configurations, focusing on both single-passenger and six-passenger UAM vehicle concepts. Their analysis revealed that blade–vortex interactions (BVI) between laterally adjacent rotors are dominant sources of far-field tonal noise. Specifically, the single-passenger configuration exhibited a maximum A-weighted SPL increase in 5 dB relative to an isolated rotor case, while the six-passenger concept produced a 14 dB higher overall sound pressure level (OASPL), underscoring the influence of rotor size and system scale on acoustic performance.

Zarri *et al.*[184] extended the study by de Vries *et al.*[94] by focusing on aeroacoustics in a three-propeller system in SBS configuration. The research primarily focuses on the deformation of helical vortical structures generated at the blade tips due to aerodynamic interactions, which result in significant variations in blade loading and subsequent noise emissions. Using LBM-VLES and Farassat's Formulation 1A, they showed that non-zero relative phase angles between propellers reduce unsteady thrust and tonal noise by up to 4.2 dB, with minimal impact on thrust.

Nargi *et al.*[95] investigated the aeroacoustic characteristics of side-by-side rotors, revealing that rotor interaction reduces thrust and torque while increasing aerodynamic load variations by up to 20%. The interaction wakes, characterized by wave-like motions and coherent vortical structures, contribute to higher OASPL. The authors further combined time-resolved particle image velocimetry (TR-PIV), proper orthogonal decomposition (POD), and wavelet transform (WT) to provide detailed insights into these interactions, though their study was limited to a fixed rotor distance and hover flight phase.

Sagaga and Lee[185] investigated overlapping SBS rotor configurations, where negative tip-to-tip spacing results in $d_y \leq 2R_p$. Their simulations demonstrated that partial overlaps of 15%–25% of the propeller radius led to substantial acoustic penalties, with SPLs exceeding freeway and community noise thresholds by approximately 20–30 dB, respectively. The increased overlap was correlated with increased unsteady aerodynamic interactions and associated noise emissions.

In a follow-up study of the full vehicle with fuselage,[186] the authors showed that tonal noise for small overlaps (0–5%) appeared at both even and BPF harmonics, indicating contributions from both rotor–rotor and rotor–upwash interactions. In contrast, larger overlaps (15%–25%) produced tonal components restricted to even harmonics, consistent with dominant BVI mechanisms. Furthermore, the relative acoustic contributions from rotors and fuselage became more balanced as the overlap increased. Notably, in select SBS configurations with fuselage, a net reduction of 3–5 dBA was achieved, suggesting the potential overlap benefits for noise. This observation highlights the need to consider the full vehicle in studies in order to obtain a realistic estimation of the vehicle's aeroacoustics.

Additionally, Celik *et al.*[187,188] experimentally demonstrated that propeller separation distance and advance ratio significantly influence both tonal and broadband noise. The study found that high-frequency broadband noise increased similarly in both hover and edgewise flight, while low-frequency broadband noise was more sensitive to changes in advance ratio and propeller separation. It was also observed that increasing the advance ratio resulted in higher low-frequency noise

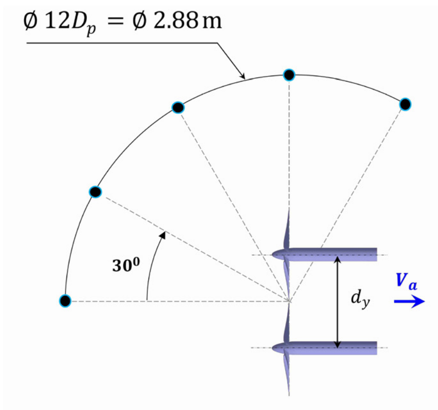

(a)

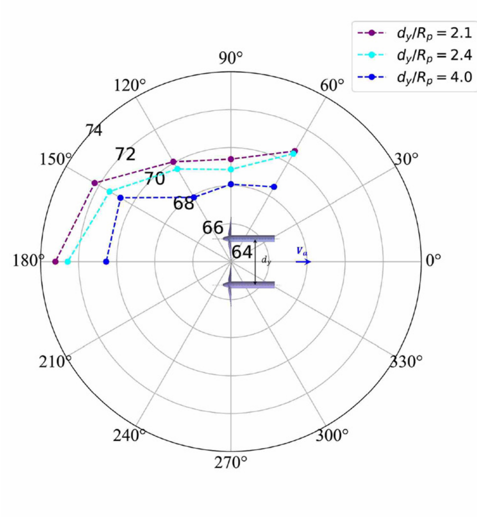

(b)

FIG. 22. Effects of lateral spacing on sound pressure level (SPL) for side-by-side (SBS) propeller configuration in hover: (a) microphone positions and (b) SPL directivity. Data extracted from Ref. 98.

across a broader bandwidth for SBS propellers, referred to by the authors as tandem configurations. At $d_y = 2.2R_p$, the noise level was higher, while it decreased at $d_y = 2.6R_p$. However, the noise level at $d_y = 2.6R_p$ was unexpectedly lower than at $d_y = 3R_p$, which the authors did not explain, suggesting that further detailed flow field analysis is needed to fully understand the underlying aeroacoustics interactions.

Moreover, numerical simulations conducted by Li *et al.*,[37] on a full hexacopter configuration, highlight the dependency of noise on rotor interactions and the significant role of arms in load fluctuations that impact OASPL. Their study suggests that extending the arms to reduce rotor interference can mitigate noise, with the fuselage contributing negligibly to overall noise levels, suggesting an optimal reference for fuselage placement and geometry for this type of vehicle. The authors confirmed that rotor–rotor interactions lead to notable thrust fluctuations and increased tonal noise, emphasizing the importance of considering these factors in the design of UAM vehicles to optimize both aerodynamic performance and noise reduction.

A recent study by Zarri *et al.*[189] emphasized the influence of propeller–propeller acoustic interference on the spatial directivity of radiated sound. The authors demonstrated that implementing phase synchronization between adjacent propellers misaligns their wakes, thereby reducing vortex interactions. This wake misalignment enables destructive acoustic interference, leading to tonal noise reductions of up to 7.5 dB (at 30° phase angle) without adversely affecting aerodynamic performance. This aligns with the findings of Turhan *et al.*,[190] who reported that a noise reduction of up to 8 dB can be achieved using two-bladed propellers with a 90° phase angle. These results suggest that coordinated propeller phasing strategies may offer a viable pathway for noise mitigation in multirotor UAM configurations.

Collectively, these studies demonstrate that SBS propeller noise is highly sensitive to lateral spacing and propeller overlap, with both tonal and broadband components significantly influenced by geometric parameters and flight conditions. Dominant noise-generating mechanisms include blade–vortex interactions, tip–vortex interference, and unsteady loading due to the propeller–propeller interaction, especially prominent in configurations with small separation. Precise propeller placement and system-scale optimization are therefore crucial to minimize acoustic penalties, which is essential for UAM operations in noise-sensitive urban environments.

While recent studies have explored phase synchronization in SBS propeller configurations as a potential noise mitigation strategy,[189] its systematic implementation and optimization across full multirotor arrays remain underexplored. The growing interest in compact multirotor architectures that combine one-after-another (OAA) and side-by-side (SBS) configurations further underscores the need for detailed experimental and computational investigations to quantify radiated noise and evaluate the effectiveness of synchronization techniques. Although significant progress has been made in multirotor aeroacoustics through high-fidelity computational fluid dynamics (CFD), computational aeroacoustics (CAA), and wind tunnel testing, full-scale vehicle noise assessments remain relatively limited. Notable contributions by Sagaga *et al.*[186] and Li *et al.*[37] have begun to address this challenge. However, the considerable computational and experimental costs associated with modeling or measuring complete vehicle configurations highlight the need for more generalized and scalable frameworks for urban noise evaluation.

In addition to propeller–propeller interactions, propeller–wing coupling introduces further acoustic complexity. For instance, in eVTOL designs incorporating lifting surfaces, such as the Joby S4[61] and Vertical Aerospace VX4,[72] propeller–wing interactions can significantly affect the overall acoustic footprint. These coupled effects are often overlooked in isolated propeller studies, yet may substantially contribute to the perceived noise signature at the system level. The aeroacoustic implications of propeller–wing interactions will therefore be analyzed in Sec. IV C.

C. Propeller–wing aeroacoustics interaction

As previously discussed, the complex flow phenomena produced by the interactions between the propellers and the wing produces changes in the aerodynamic performance of both components of a eVTOL vehicle. The said changes in performance also imply changes in the aeroacoustic footprint of the vehicle. The unsteady phenomena observed both over the propeller and wing pressure distributions cause and increase in tonal noise,[147] that may radiate not only from the propeller blades but also from the wing surface. Moreover, the ingestion of turbulent flow by the propeller in some configurations generates an increase in the broadband noise produced by the propeller. On the other hand, the existence of large surfaces like wings near the main noise sources (the propellers) contributes to the emergence of reflections and diffraction of sound waves that change the directivity of the noise.[191,192]

Akiwate *et al.*[193] analytically investigated the noise generated by a propeller–wing configuration. A model was developed to study the acoustic emissions of propeller wing systems. Viscous-wake, potential-field, and tip–vortex noise were considered the main tonal sources due to propeller–wing interactions, whereas wake interactions were considered the main contribution to broadband noise. It was found that noise emissions depend not only on the separation between the propeller and the wing but also on the number of blades and other geometrical factors. Moreover, at low tip Mach values it was found that interaction noise sources dominated above propeller-only noise. This preliminary study proves that the acoustic footprint of a propeller–wing system is influenced by several geometrical factors and interactions that noticeably change the noise.

Zawodny *et al.*[147] used a combination of experimental measurements and numerical simulations using CFD and the FW–H analogy to study the influence of the propeller position on the radiated sound. Variations in the directivity of the BPF noise were reported even for small variations in the wing position. Furthermore, for some positions a low noise region was observed after the propeller plane. The numerical simulations showed that the propeller and the wing were both important noise sources at the blade passing frequency, with the wing being the main contributor downstream the plane of rotation. This confirms the importance of taking into account the propeller–wing interactions not only because of the influence of the wing over the propeller pressure distribution but also because the wing surface can effectively contribute to the noise generated.

Wickersheim *et al.*[192] studied the acoustic characteristics of three co-rotating propellers placed upstream a wing in high-lift configuration in climb condition. It was found that both the propellers and the wing system are relevant noise sources, with the dominant one being either of the two depending on the angle of the observer. The use of permeable and impermeable FW–H surfaces was also evaluated, concluding that the use of impermeable surfaces is a valid approach. The scattering effects at the wing surfaces were also studied with a FW–H + BEM approach, and the importance of the acoustic shielding effect of big surfaces near the propellers was demonstrated.

In addition to conventional fixed-propeller wing configurations, emerging UAM concepts such as vectored-thrusts introduce aeroacoustic source mechanisms that are not yet fully understood. In this context, Chaitanya *et al.*[194] experimentally studied a tiltrotor–wing during different flight phases. Figure 23 illustrates the flow distortion and noise sources generated by the interaction of the propeller wake with the wing surface during the vertical takeoff/hover phase. Under these conditions, the study reported similar trend in the directivity of the OASPL or tonal noise; however, the propeller–wing interaction was found to noticeably influence the acoustic signature compared to the isolated propeller, depending on the propeller's relative position. Moreover, the interaction between the propeller tip vortex and the wing was identified as a relevant noise source during transition, when the propeller is positioned at 45° relative to the wing.

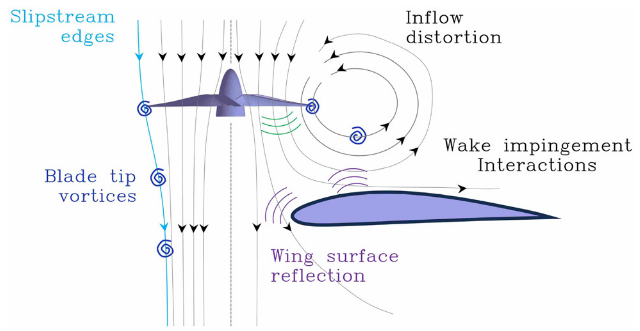

FIG. 23. Sketch of noise sources on a propeller–wing configuration in hover conditions.

In over-the-wing and pusher configurations, Zaman *et al.*[195] experimentally investigated the noise emissions of a propeller ingesting turbulent boundary layers of varying thickness. Broadband noise emissions increased in direct correlation with boundary layer thickness. The size of turbulent structures within the boundary layer influenced the frequency at which this effect manifests. Moreover, the broadband noise increase was more pronounced downstream of the propeller, effectively altering noise directivity. Regarding tonal noise, the thickness and intensity of the turbulent boundary layer significantly affect the magnitude of the first harmonic of the blade passing frequency (BPF), with differences up to 10 dB.

These studies illustrate the relevance of propeller–wing interactions on the acoustic emissions of UAM vehicles, as well as their dependence on the relative positioning of the two components. However, the nature and magnitude of these interactions still require further investigation in order to develop proper guidelines for reducing the acoustic footprint of eVTOL vehicles.

Moreover, numerical models are required to evaluate multiple design configurations within acceptable computational time. Low-order aerodynamic methods such as BEMT, vortex lattice method (VLM), and vortex particle method (VPM) are attractive because they provide rapid estimates of thrust, torque, and the dominant tonal components (at least the first blade-passing frequency) for isolated propellers when coupled with acoustic analogies such as the Ffowcs-Williams and Hawkings (FW–H) formulation. However, these methods rely on simplifying assumptions, including axisymmetric inflow, inviscid flow, prescribed or frozen wakes, neglected turbulence structures, and the compact acoustic-source assumption, which inherently limit their predictive accuracy.[167,196] As a result, they are unable to adequately capture key flow physics such as propeller–propeller and propeller–wing interactions, turbulence ingestion, and swirl flow, and they cannot accurately predict higher-order harmonics or high-frequency broadband noise. Higher-fidelity CFD-based methods, including unsteady RANS (URANS), large-eddy simulation (LES), lattice-Boltzmann method very large-eddy simulation (LBM-VLES), and hybrid CFD–CAA approaches (e.g., unsteady CFD coupled with FW–H), provide more accurate predictions of unsteady aerodynamic loading and broadband acoustic sources, but at significantly increased computational expense. This motivates the development of reduced-order CFD tools, such as the framework by Cheng *et al.*,[197] as well as multi-fidelity workflows, which combine low- and high-fidelity methods to reduce computational cost while improving predictive capability.

Table VIII summarizes the main low-order and CAA-based approaches used for propeller noise prediction, including their key assumptions, limitations, and computational cost. To predict propeller noise, acoustic analogy formulations require aerodynamic inputs, such as unsteady surface pressures, blade loading distributions, wake characteristics, or volumetric flow quantities.[198] These inputs are typically obtained from CFD solvers, vortex–wake methods, or other aerodynamic models. For simplicity, the FW–H formulation[199] is presented as the representative acoustic analogy, as it is the most widely applied method for propeller and rotor noise prediction. It is frequently solved using time-domain discretization, such as Farassat formulation 1A.[200] Some semi-empirical models, such as Amiet's trailing-edge model[201] and Hanson's formulation,[202] are also widely used for propeller noise prediction. These methods reliably predict both tonal and broadband noise mechanisms in multirotor systems.

D. Psychoacoustics of multirotor noise

Propeller noise in UAM literature has predominantly been characterized using spectral distributions and overall sound pressure levels (OASPL, dB) or A-weighted levels [dB(A)] to account for human hearing sensitivity. However, these energy-based metrics do not fully capture auditory perception and often correlate poorly with subjective annoyance. Psychoacoustic sound-quality metrics (SQMs), including loudness, tonality, sharpness, fluctuation strength, and roughness, are formally defined in Ref. 204. These metrics can be combined into the psychoacoustic annoyance (PA) index, providing a quantitative measure of perceived noise impact on humans.[205]

In multirotor configurations, acoustic interactions modify both discrete harmonic components and broadband content. Experimental studies on contra-rotating propellers have shown that decreasing propeller spacing increases OASPL and simultaneously increases psychoacoustic annoyance due to higher loudness and tonality, whereas increasing spacing reduces both OASPL and SQMs.[206,207] These results reported that interaction-induced tonal peaks dominate perceived sound quality relative to broadband levels alone. SQMs are more sensitive to spectral shape, particularly harmonic content and modulation, than to OASPL. Importantly, reductions in OASPL do not necessarily correspond to reductions in perceived loudness. SQM weighting functions emphasize the mid-frequency region (1–5 kHz), where human auditory sensitivity is highest, while being less affected by low- and high-frequency components.[204] Consequently, multirotor configurations that redistribute acoustic energy toward frequency bands with lower auditory sensitivity may exhibit lower psychoacoustic metrics despite similar or even higher OASPL, whereas energy shifted into mid-frequency bands can increase perceived annoyance.

Propeller interactions with neighboring components, including adjacent propellers or lifting surfaces, can intensify blade–vortex interaction (BVI) and blade–wake interaction (BWI) phenomena, thereby amplifying discrete tonal components within the radiated acoustic spectrum.[98,194,206] These tonal peaks are directly linked to tonality, which quantifies the degree to which a sound is perceived as tonal.[205] Tonal content is generally perceived as more annoying than

TABLE VIII. Comparison of typical propeller noise prediction methods for multirotor systems. Methods are ordered from low- to high-fidelity, with key assumptions, applicability, limitations, and computational cost.

Method	Key assumptions	Applicability	Key limitations	Computational cost
BEMT + FW–H[167]	Axisymmetric inflow; uniform induced velocity; steady; no wake dynamics	Isolated propeller performance (thrust, torque); tonal noise (first blade-passing frequency)	Cannot resolve unsteady loading; neglects multirotor interactions and turbulence ingestion; inaccurate broadband noise	Low
VLM/VPM + FW–H[96,128,132,196]	Vortex-based aerodynamic modeling; attached flow; dynamic Lagrangian/free wake or prescribed/simplified wake	Wake interactions; basic tonal noise prediction; approximate induced velocities	Limited wake resolution; no direct turbulence modeling; limited broadband fidelity; acceptable (but less accurate) for multirotor interactions	Low–medium
URANS + FW–H[203]	Time-averaged RANS turbulence; unsteady inflow	Propeller inflow distortion, unsteady pressures; some broadband noise; suitable for multirotor interactions	Cannot fully resolve high-frequency broadband noise; expensive for multirotor interactions	Medium–high
LES/LBM-VLES + FW–H[189]	Resolves large-scale turbulence; Sub-Grid Scale or particle-based model; fully unsteady	Unsteady wakes; turbulence ingestion; tonal and broadband noise; suitable for multirotor interactions	High computational cost; domain size limited	High–very high

broadband noise at the same overall level. Tonal components at very low frequencies (typically below 200 Hz) are often perceived as pressure, or vibration rather than an audible pitch, potentially causing discomfort.[208] Sharpness, associated with high-frequency content, further contributes to perceived unpleasantness when combined with elevated tonality. Roughness and fluctuation strength quantify temporal modulations of the acoustic signal, with roughness corresponding to rapid amplitude variations perceived as harshness, and fluctuation strength to slower periodic modulations.[205]

Therefore, for UAM vehicle configurations, assessments based solely on acoustic energy-based metrics may be misleading. Incorporating psychoacoustic sound-quality metrics (SQMs) such as loudness, tonality, and fluctuation strength, in addition to OASPL or A-weighted sound pressure levels, provides a more accurate representation of perceived annoyance and potential community impact.

V. DESIGN IMPLICATIONS FOR UAM VEHICLES

The integration of multirotor eVTOL aircraft into urban environments presents a unique set of design challenges and trade-offs, especially concerning aerodynamic efficiency and noise emissions. The insights gained from the review of propeller–propeller and propeller–wing aerodynamic and aeroacoustic interactions provide critical guidance for addressing these challenges. This section outlines key implications of the analyzed findings for propeller system configurations and vehicle architecture, which are essential for viable urban air mobility (UAM) deployment. The aerodynamic and aeroacoustic characteristics of multirotor configurations directly inform eVTOL design choices for UAM applications

One of the most consequential design decisions in multirotor eVTOLs is the spatial arrangement of the propellers. Experimental and numerical studies on the propellers alone (without the wing or the fuselage) show that:

1. In multirotor configuration, thrust losses of the propeller that is located within the wake of another propeller can reach up to 80% compared to isolated propeller, depending on axial and lateral spacing, operating conditions, and propellers geometrical characteristics.
2. In the one-after-another configuration, maintaining a lateral spacing greater than $2R_p$ is crucial to limit the reduction in aerodynamic performance to less than 4%. This spacing minimizes aerodynamics interaction between the propellers, thereby preserving their individual performance characteristics. At this lateral spacing, the influence of axial spacing becomes negligible.
3. When propellers are arranged side-by-side configuration, in forward flight or vertical flight, i.e., propellers aligned with flight direction, the aerodynamic performance loss is generally limited to less than 3%, indicating minimal aerodynamics drawbacks in using a distributed electric propulsion system. However, in non-axial inflow, the thrust losses of the rear propeller can reach up to 30%,[35] reducing efficiency and increasing unsteady blade loading.
4. Based on the analysis of propeller–wing aerodynamic interactions across multiple configurations representative of UAM vehicle architectures, the following design considerations are identified:
5. Tractor configuration can increase lift by re-energizing the flow over the wing surface. For a single tractor propeller, the lift coefficient can increase by up to 34%[140] compared to a clean wing. The degree of benefit is influenced by the number of propellers and their rotational direction as the components geometries. However, this configuration also introduces strong unsteady pressure fields on the wing due to the impingement of the propeller slipstream. While pusher configurations can also enhance lift, they tend to generate more turbulent wake interactions and suffer from reduced L/D ratios. Nevertheless, boundary layer ingestion in these configurations may improve propeller efficiency in some cases, though the blades encounter highly nonuniform inflow.
6. Over-the-wing (OTW) configuration can accelerate the flow over the upper wing surface, resulting in a substantial improvement in lift-to-drag (L/D) ratio, reported to be higher than that of baseline tractor configurations for a single propeller–wing configuration primarily due to significant drag reduction, as the increase in lift is relatively minor (approximately 1.3%).[97] However, OTW placement may also induce localized flow separation and complex vortex shedding, particularly when propeller blade tips interact with the wing boundary layer, potentially degrading propulsive efficiency. In contrast, under-the-wing (UTW) configurations can provide some aerodynamic benefits but often require increased landing gear height to maintain sufficient ground clearance, introducing practical integration challenges.
7. Wingtip-mounted propellers, especially in inboard-up rotating configurations, can suppress wingtip vortex formation, reducing induced drag and potentially improving both. These configurations may be deployed in either tractor or pusher modes. Their effectiveness, however, is highly sensitive to boom length and propeller rotational direction, which govern the extent of vortex–propeller interaction and the resulting distribution of tonal and broadband noise in the far field.
8. Unlike aerodynamic performance metrics, which are intrinsic to a given vehicle configuration, aeroacoustic emissions are highly sensitive to both configuration and observer location, and are further modulated by acoustic propagation and environmental effects. Therefore, conclusions drawn from aerodynamic analyses cannot be directly generalized to the noise emission. Both OAA and SBS configurations induce unsteady aerodynamic loading due to propeller–wake interactions, inflow distortion, and blade–vortex interactions. These phenomena generate both tonal and broadband noise components, stemming from turbulence ingestion and dynamic blade responses. Notably, closer propeller spacing intensifies these interactions, leading to increased noise levels:
9. In OAA configurations, co-rotating propellers (i.e., rotating in the same direction) should be favored over counter-rotating, as the latter have been shown to slightly increase noise levels (up to 2.6 dB). During hover, for an observer positioned at a distance of $12R_p$ from the system center, a two-propeller configuration with axial and lateral spacings of $d_x = 0.5R_p$ and $d_y = 2R_p$, respectively, exhibits lower noise compared to smaller spacings. Further increasing the spacing results in only a marginal noise reduction of approximately 0.8 dB.[127]

10. In SBS configuration, phase synchronization between propellers can reduce noise level by up to 7.5 dB, depending on propeller number, geometry, and observer location. Phase control is especially effective in reducing coherent pressure fluctuations that contribute to prominent tonal peaks in the frequency spectrum.
11. Although propeller–wing aerodynamic interactions can, in some cases, improve overall performance metrics such as lift-to-drag ratio (L/D) and propulsive efficiency (η_p), they often introduce acoustic penalties. These penalties are primarily driven by noise mechanisms arising from wake impingement and unsteady surface pressure fluctuations on both the wing and the rotating blades. Maintaining adequate clearance between the propeller and adjacent aerodynamic surfaces is strongly recommended to mitigate these effects.

A single, isolated propeller can generate sound pressure levels (SPLs) up to 85 dB in hover conditions,[127] but integration within a vehicle architecture can further amplify these levels due to wake interactions and combined aerodynamic effects. Compliance with the expected, target urban operational noise limits, particularly during takeoff and approach phase, represents a significant design challenge. Addressing this challenge requires a multifaceted approach that combines geometric configuration and operational noise mitigation strategies. High-efficiency electric propulsion enables maintaining thrust while reducing blade tip velocities, contributing to reductions in both broadband and tonal speed. In addition, alternative blade designs, including joined-blade configurations[209,210] and serrated blades,[211–213] can be explored to assess their potential noise reduction benefits. Overall, these considerations highlight the importance of an integrated approach to aerodynamic and aeroacoustic design in multirotor systems, particularly for urban air mobility operations where vehicles must operate in densely populated and noise sensitive environments.

VI. CONCLUSIONS

The rapid advancement of UAM and the increasing focus on electric vertical takeoff and landing (eVTOL) aircraft represent a transformative shift in urban transportation. As urban environments become more congested and ground transportation systems reach their limits, the integration of UAM offers a compelling solution to enhance mobility, reduce travel times, and decrease environmental impacts. However, the successful deployment of eVTOL aircraft in urban airspace hinges on overcoming significant technical challenges, particularly those related to the aerodynamics and aeroacoustics of multirotor configurations. This review has highlighted the critical interactions between propeller–propeller and propeller–wing in multirotor eVTOL designs, revealing both the benefits and challenges of these configurations. The analysis shows that distributed electric propulsion in side-by-side propeller arrangements results in minimal thrust loss, typically less than 3%. This indicates that aerodynamic performance is largely preserved. However, the fluctuation in propeller loading poses a significant challenge, as it leads to increased noise levels, which is a critical factor in the acceptance and integration of UAM systems in densely populated urban areas. Additionally, the study underscores the importance of propeller spacing and phase synchronization in minimizing aerodynamic penalties and noise generation. In one-after-another configurations where one propeller is positioned directly behind another, the rear propeller must maintain a lateral separation of at least twice the propeller radius to achieve performance within 4% of an isolated propeller. To minimize interaction noise, an axial spacing of at least half of the propeller radius, combined with a lateral spacing of at least twice the propeller radius, may be required. For propeller–wing interactions, tractor and over-the-wing configurations generally offer better aerodynamic efficiency compared to other arrangements; however, wake impingement on the wing causes loading fluctuations and increase noise levels. These findings are crucial for designing eVTOL aircraft that are both efficient and compliant with stringent urban noise regulations. The studies have also demonstrated that, under the same operating conditions, the interaction effects vary depending on the specific propeller geometry and operating conditions.

Despite the progress in multirotor eVTOLs aerodynamics and aeroacoustics, some extensive research are still needed:

1. Three-dimensional spacing in OAA configurations: Most studies OAA configurations focus on two propellers with planar spacing in axial and lateral directions (d_x, d_y). However, practical multirotor eVTOL configurations often involve three or more propellers arranged in complex three-dimensional layouts, making vertical spacing (d_z) equally important. There is a clear need for detailed investigations involving at least three interacting propellers in OAA configurations, assessing both aerodynamic and aeroacoustic interactions.
2. Non-axial inflow during transition phases: The transition phase such as during the shift from vertical to horizontal flight or vice versa introduces highly non-axial inflow conditions, particularly in tiltrotor and tilt-wing configurations. Existing aeroacoustic studies remain limited, especially for SBS and OAA propeller configurations where the propeller axes align with the flight direction (incoming flow). Comprehensive investigations that quantify noise emissions across the full tilt range (e.g., from 0° to 90°) are still needed.
3. Dynamic motion of tiltrotors: Most aerodynamic studies of transition phases evaluate propeller performance at discrete, static tilt angles, overlooking the effects of continuous motion. In reality, transitions occur over short time scales, during which flow unsteadiness, vortex shedding, and blade–vortex interactions can cause significant aerodynamic and aeroacoustic penalties. High-fidelity investigations that capture unsteady aerodynamics and noise generation during continuous, time-dependent tilting are therefore critically needed, rather than relying solely on static-angle analyses.
4. In-wing embedded configuration: Some recent UAM concepts incorporate in-wing embedded propellers, where the propeller disk is integrated into the wing structure. These configurations can alter both aerodynamic efficiency and acoustic radiation characteristics. The performance of such systems remains largely unexplored and requires dedicated investigation.
5. Fluid–structure interaction and vibroacoustics: The impact of unsteady loading from propeller–propeller interactions on structural response remains underexplored. Future research should also focus on high-fidelity fluid–structure interaction (FSI) and vibroacoustic analyses to understand how unsteady aerodynamic forces induce blade vibrations, structural fatigue, and structure-borne noise, which can significantly affect vehicle longevity and community noise levels.

6. Parametric studies on propeller–wing separation: Detailed parametric studies quantifying how propeller–wing separation distance affects both aerodynamic efficiency and noise generation are still needed.
7. Propeller–wing interactions with control surfaces: Most studies assume clean, static wing surfaces. However, UAM wings often include control surfaces, and the effects of turbulent, high-velocity propeller inflow on these surfaces, particularly on unsteady loading and noise generation, remain poorly understood, especially during transition or maneuvering.
8. Full-vehicle aerodynamic and aeroacoustic assessment: While isolated component studies provide valuable insight into subsystem behavior, they do not fully capture the coupled aerodynamic and aeroacoustic interactions present in multirotor eVTOL aircraft. Future investigations should therefore focus on full-vehicle validation, supported by high-fidelity simulations and experimental testing, even at increased computational and experimental cost, to obtain reliable performance and noise predictions for operational UAM environments.

The present review establishes a foundational framework for addressing the key aerodynamic and aeroacoustic challenges associated with multirotor systems and highlights critical gaps in the existing literature. By addressing these gaps, implementing the recommended design strategies, and validating full-vehicle configurations, future research can advance multirotor technology while ensuring the safe, efficient, and community acceptable integration of eVTOL aircraft into urban airspace.

ACKNOWLEDGMENTS

The authors wish to express their sincere gratitude to the researchers whose work in the fields of urban air mobility, multirotor aerodynamics, and aeroacoustics has greatly informed and enriched this review. Their valuable contributions in terms of data, findings, and insights have been instrumental in shaping the discussions and conclusions presented herein.

The authors also gratefully acknowledge the support of the Renewable Energies and Advanced Materials Laboratory (LERMA).

F. N. Ramírez is supported by Grant No. PREP2022-000221 funded by MICIU/AEI/10.13039/501100011033 and by "ESF Investing in your future."

AUTHOR DECLARATIONS

Conflict of Interest

The authors have no conflicts to disclose.

Author Contributions

Kangni Combey: Conceptualization (equal); Data curation (equal); Formal analysis (equal); Investigation (equal); Methodology (equal); Writing – original draft (equal); Writing – review & editing (equal). **Omer A. Elsayed:** Conceptualization (supporting); Supervision (equal); Writing – review & editing (equal). **Andrea Magrini:** Conceptualization (equal); Investigation (equal); Writing – original draft (equal); Writing – review & editing (equal). **Federico N. Ramirez:** Investigation (equal); Writing – original draft (equal). **Sen Wang:** Investigation (equal); Writing – original draft (equal). **Khaoula Qaissi:** Supervision (equal); Writing – review & editing (equal). **Hajar Chouiyakh:** Supervision (equal); Writing – review & editing (equal). **Lourenco T. L. Pereira:** Conceptualization (equal); Supervision (equal); Writing – original draft (equal); Writing – review & editing (equal). **Daniele Ragni:** Conceptualization (equal); Supervision (equal); Writing – review & editing (equal).

DATA AVAILABILITY

Data sharing is not applicable to this article as no new data were created or analyzed in this study.

REFERENCES

[1] NASA, "Urban air mobility" (2025). https://plus.nasa.gov/video/urban-air-mobility/ (accessed May 14, 2025).
[2] Eve Air Mobility, "Brand center" (2025). https://www.eveairmobility.com/brand-center/ (accessed December 12, 2025).
[3] Jeff Holden and Nikhil Goel, "Fast-forwarding to a future of on-demand urban air transportation" (2016). https://evtol.news/__media/PDFs/UberElevateWhitePaperOct2016.pdf (accessed June 30, 2025).
[4] G. Palaia, K. A. Salem, V. Cipolla, V. Binante, and D. Zanetti, "A conceptual design methodology for e-VTOL aircraft for urban air mobility," Appl. Sci. **11**(22), 10815 (2021).
[5] N. Polaczyk, E. Trombino, P. Wei, and M. Mitici, "A review of current technology and research in urban on-demand air mobility applications," in *8th Biennial Autonomous VTOL Technical Meeting and 6th Annual Electric vTOL Symposium* (Vertical Flight Society, Mea, AZ, 2019), pp. 333–343.
[6] A. Bauranov and J. Rakas, "Designing airspace for urban air mobility: A review of concepts and approaches," Prog. Aerosp. Sci. **125**, 100726 (2021).
[7] RTL Nieuws, "Ambulance vaak te laat: Wachttijden bij spoedhulp in steden lopen op" (2025). https://www.rtl.nl/nieuws/onderzoek/artikel/5493952/noodhulp-112-hulpdienst-aanrijtijden-wachten-ambulance (accessed May 2, 2025).
[8] A. Cohen and S. Shaheen, "Urban air mobility: Opportunities and obstacles," in *International Encyclopedia of Transportation* (UC Berkeley, 2021), pp. 702–709.
[9] A. P. Cohen, S. A. Shaheen, and E. M. Farrar, "Urban air mobility: History, ecosystem, market potential, and challenges," IEEE Trans. Intell. Transp. Syst. **22**(9), 6074–6087 (2021).
[10] L. Wang, X. Deng, J. Gui, P. Jiang, F. Zeng, and S. Wan, "A review of urban air mobility-enabled intelligent transportation systems: Mechanisms, applications and challenges," J. Syst. Archit. **141**, 102902 (2023).
[11] J. Shi, P. Cong, L. Zhao, X. Wang, S. Wan, and M. Guizani, "A two-stage strategy for UAV-enabled wireless power transfer in unknown environments," IEEE Trans. Mob. Comput. **23**(2), 1785–1802 (2023).
[12] M. Heidet, K. H. Benjamin Leung, W. Bougouin, R. Alam, B. Frattini, D. Liang, D. Jost, V. Canon, J. Deakin, H. Hubert *et al.*, "Improving EMS response times for out-of-hospital cardiac arrest in urban areas using drone-like vertical take-off and landing air ambulances: An international, simulation-based cohort study," Resuscitation **193**, 109995 (2023).
[13] N. Gunady, B. E. Sells, S. R. Patel, H. Chao, D. A. DeLaurentis, and W. A. Crossley, "Evaluating future electrified UAM-enabled middle-mile cargo delivery operations," in *AIAA Aviation 2022 Forum* (AIAA, 2022).
[14] D. Gillis, M. Petri, A. Pratelli, I. Semanjski, and S. Semanjski, "Urban air mobility: A state of art analysis," in *Computational Science and Its Applications—ICCSA 2021: 21st International Conference*, Cagliari, Italy, September 13–16, 2021 (Springer, 2021), pp. 411–425.
[15] V. Garg, S. Niranjan, V. Prybutok, T. Pohlen, and D. Gligor, "Drones in last-mile delivery: A systematic review on efficiency, accessibility, and sustainability," Transp. Res. Part D: Transp. Environ. **123**, 103831 (2023).
[16] X. Li, J. Tupayachi, A. Sharmin, and M. M. Ferguson, "Drone-aided delivery methods, challenge, and the future: A methodological review," Drones **7**(3), 191 (2023).
[17] Michael Shamiyeh, Raoul Rothfeld, and Mirko Hornung, "A performance benchmark of recent personal air vehicle concepts for urban air mobility," in

Proceedings of the 31st Congress of the International Council of the Aeronautical Sciences, Belo Horizonte, Brazil (ICAS, 2018). https://www.icas.org/ICAS_ARCHIVE/ICAS2018/data/papers/ICAS2018_0794_paper.pdf.
[18]S. Rajendran and J. Shulman, "Study of emerging air taxi network operation using discrete-event systems simulation approach," J. Air Transp. Manage. **87**, 101857 (2020).
[19]L. A. Garrow, B. German, P. Mokhtarian, and J. Glodek, "A survey to model demand for eVTOL urban air trips and competition with autonomous ground vehicles," in *AIAA Aviation 2019 Forum* (AIAA, 2019).
[20]L. Swadesir and C. Bil, "Urban air transportation for melbourne metropolitan area," in *AIAA Aviation 2019 Forum* (AIAA, 2019).
[21]T. Mercan, V. Yavas, D. Can, and Y. Mercan, "Vertiport location selection criteria for urban air mobility," J. Air Transp. Manage. **124**, 102760 (2025).
[22]K. Schweiger and F. Knabe, "Vertidrome airside level of service: Performance-based evaluation of Vertiport airside operations," Drones **7**(11), 671 (2023).
[23]H. D. Kim, A. T. Perry, and P. J. Ansell, "A review of distributed electric propulsion concepts for air vehicle technology," in *2018 AIAA/IEEE Electric Aircraft Technologies Symposium (EATS)* (IEEE, 2018), pp. 1–21. https://ntrs.nasa.gov/citations/20180004729.
[24]Hyun Dae Kim, Aaron T. Perry, and Phillip J. Ansell, "Progress in distributed electric propulsion vehicles and technologies," Technical Report 20200011461 (2020).
[25]B. J. Brelje and J. R. Martins, "Electric, hybrid, and turboelectric fixed-wing aircraft: A review of concepts, models, and design approaches," Prog. Aerosp. Sci. **104**, 1–19 (2019).
[26]C. Courtin, A. Mahseredjian, A. J. Dewald, M. Drela, and J. Hansman, "A performance comparison of eSTOL and eVTOL aircraft," in *AIAA Aviation 2021 Forum* (AIAA, 2021).
[27]N. K. Borer, M. D. Patterson, J. K. Viken, M. D. Moore, J. Bevirt, A. M. Stoll, and A. R. Gibson, "Design and performance of the NASA sceptor distributed electric propulsion flight demonstrator," in *16th AIAA Aviation Technology, Integration, and Operations Conference* (AIAA, 2016).
[28]A. Omar Tiseira Izaguirre, L. M. García-Cuevas González, P. Q. Igeño, and P. Varela Martínez, "Series-hybridisation, distributed electric propulsion and boundary layer ingestion in long-endurance, small remotely piloted aircraft: Fuel consumption improvements," Aerosp. Sci. Technol. **120**, 107227 (2022).
[29]D. Planas Andrés, E. Nguyen Van, C. Döll, and P. Pastor, "Multi-disciplinary optimization of a distributed electric propulsion aircraft under aero-propulsive effects," CEAS Aeronaut. J. **16**, 571–589 (2025).
[30]B. Ren, C. Yang, X. Zhang, and W. Mao, "Modeling and switched control of modular reconfigurable flight array for faulty redundancy," Processes **12**(4), 646 (2024). https://www.mdpi.com/2227-9717/12/4/646.
[31]M. T. Fard, J. He, H. Huang, and Y. Cao, "Aircraft distributed electric propulsion technologies—A review," IEEE Trans. Transp. Electr. **8**(4), 4067–4090 (2022).
[32]K. A. Deere, S. Viken, M. Carter, J. K. Viken, M. Wiese, and N. Farr, "Computational analysis of powered lift augmentation for the Leaptech distributed electric propulsion wing," in *35th AIAA Applied Aerodynamics Conference* (AIAA, 2017).
[33]J. Alba-Maestre, K. Prud'homme van Reine, T. Sinnige, and S. G. P. Castro, "Preliminary propulsion and power system design of a tandem-wing long-range eVTOL aircraft," Appl. Sci. **11**(23), 11083 (2021).
[34]A. Zanotti, "Experimental study of the aerodynamic interaction between side-by-side propellers in eVTOL airplane mode through stereoscopic particle image velocimetry," Aerospace **8**(9), 239 (2021).
[35]T. C. A. Stokkermans, D. Usai, T. Sinnige, and L. L. M. Veldhuis, "Aerodynamic interaction effects between propellers in typical eVTOL vehicle configurations," J. Aircraft **58**(4), 815–833 (2021).
[36]C. E. Tinney and J. Sirohi, "Multirotor drone noise at static thrust," AIAA J. **56**(7), 2816–2826 (2018).
[37]Y. Li, Z. Ma, P. Zhou, S. Zhong, and X. Zhang, "A numerical investigation of the aerodynamic and aeroacoustic interactions between components of a multi-rotor vehicle for urban air mobility," J. Sound Vib. **571**, 118002 (2024).
[38]W. Qu, C. Xu, X. Tan, A. Tang, H. He, and X. Liao, "Preliminary concept of urban air mobility traffic rules," Drones **7**(1), 54 (2023).
[39]J. D. Anderson, *Aircraft Performance and Design*, 1st ed. (WCB McGraw-Hill Education, New York, 2010).
[40]J. Prasad Rao, J. E. Holzsager, M. M. Maia, and J. F. Diez, "Experimental study into optimal configuration and operation of two-four rotor coaxial systems for eVTOL vehicles," Aerospace **9**, 252 (2022).
[41]R. Berger, *Hope on the Horizon: A study of the Aerostructure Tooling Market* (Roland Berger Focus, 2018). https://www.rolandberger.com/publications/publication_pdf/roland_berger_aerostructure_tooling_market.pdf (accessed May 7, 2025).
[42]J. D. Anderson, *Fundamentals of Aerodynamics*, 6th ed. (WCB McGraw-Hill Education, New York, 2011).
[43]G. J. Leishman, *Principles of Helicopter Aerodynamics with CD Extra* (Cambridge University Press, 2006). https://air.flyingway.com/faa_exam/heli/principles_of_helicopter_aerodynamics.pdf.
[44]A. Kasliwal, N. J. Furbush, J. H. Gawron, J. R. McBride, T. J. Wallington, R. D. De Kleine, H. C. Kim, and G. A. Keoleian, "Role of flying cars in sustainable mobility," Nat. Commun. **10**(1), 1555 (2019).
[45]S. Pinheiro Melo, F. Cerdas, A. Barke, C. Thies, T. S. Spengler, and C. Herrmann, "Life cycle engineering of future aircraft systems: The case of eVTOL vehicles," Procedia CIRP **90**, 297–302 (2020).
[46]Y. Fukumine and Z. Lei, "Estimation of eVTOL flight performance using rotorcraft theory," in *The 33rd Congress of the International Council of the Aeronautical Sciences (ICAS)* (ICAS, 2022). https://www.icas.org/icas_archive/ICAS2022/data/papers/ICAS2022_0408_paper.pdf.
[47]J. Zhang, Y. Liu, and Y. Zheng, "Overall eVTOL aircraft design for urban air mobility," Green Energy Intell. Transp. **3**(2), 100150 (2024).
[48]N. Qiao, T. Ma, X. Wang, J. Wang, J. Fu, and P. Xue, "An approach for formation design and flight performance prediction based on aerodynamic formation unit: Energy-saving considerations," Chin. J. Aeronaut. **37**(3), 77–91 (2024).
[49]Nabil Hagag, Felix Toepsch, Simon Graf, Michael Büddefeld, and Hugo Eduardo, "Maximum total range of eVTOL under consideration of realistic operational scenarios" (2021). https://www.sesarju.eu/sites/default/files/documents/sid/2021/papers/SIDs_2021_paper_69.pdf.
[50]A. Bacchini and E. Cestino, "Electric vTOL configurations comparison," Aerospace **6**(3), 26 (2019).
[51]F. Bohorquez, P. Samuel, J. Sirohi, D. Pines, L. Rudd, and R. Perel, "Design, analysis and hover performance of a rotary wing micro air vehicle," J. Am. Helicopter Soc. **48**(2), 80–90 (2003).
[52]W. J. F. Koning, B. N. P. Perez, H. V. Cummings, E. A. Romander, and W. Johnson, "Overview of rotor hover performance capabilities at low Reynolds number for Mars exploration," Technical Report 20240010521 (2024). https://ntrs.nasa.gov/citations/20240010521.
[53]Cahit Kitaplioglu, "Analysis of small-scale rotor hover performance data," Technical Report NASA-TM-102271 (1990). https://ntrs.nasa.gov/citations/19900011009.
[54]eVTOL Aircraft Directory, "Electric VTOL Aircraft News by The Vertical Flight Society (VFS)." https://evtol.news/aircraft (accessed May 14, 2025).
[55]S. Rajendran and S. Srinivas, "Air taxi service for urban mobility: A critical review of recent developments, future challenges, and opportunities," Transp. Res. part E: Logistics Transp. Rev. **143**, 102090 (2020).
[56]S. S. Chauhan and J. R. Martins, "Tilt-wing eVTOL takeoff trajectory optimization," J. Aircraft **57**(1), 93–112 (2020).
[57]Siena K. S. Whiteside, Beau P. Pollard, Kevin R. Antcliff, Nikolas S. Zawodny, Xiaofan Fei, Christopher Silva, and Glenn L. Medina, "Design of a tiltwing concept vehicle for urban air mobility," Technical Report TM-20210017971 (2021).
[58]Aurora lightning strike. https://www.aurora.aero/programs/ (accessed May 5, 2025).
[59]Vahana a^3 eVTOL aircraft. https://www.airbus.com/en/innovation/low-carbon-aviation/urban-air-mobility/cityairbus-nextgen/vahanaa (accessed May 5, 2025).
[60]L. Preis, M. T. Kotwicz Herniczek, and B. J. German, "Assessing prominent eVTOLs based on Vertiport throughput, noise, and speed using multi-dimensional Pareto fronts," Aerosp. Sci. Technol. **159**, 109971 (2025).
[61]Joby Aviation, "Joby S4." https://www.jobyaviation.com (accessed May 5, 2025).
[62]Bell Nexus. https://news.bellflight.com/en-US/tags/bell-nexus/ (accessed May 5, 2025).

[63]A. Jha, N. Prabhakar, D. Karbowski, and B. German, "Urban air mobility: A preliminary case study for Chicago and Atlanta," in *2022 IEEE Transportation Electrification Conference & Expo (ITEC)* (IEEE, 2022), pp. 300–306.
[64]X. Qiao, G. Chen, W. Lin, and J. Zhou, "The impact of battery performance on urban air mobility operations," Aerospace **10**(7), 631 (2023).
[65]Wisk Aero, "Kitty Hawk Cora." https://wisk.aero (accessed May 5, 2025).
[66]Beta Technologies, "Aircraft configurations." https://www.beta.team/aircraft/ (accessed May 5, 2025).
[67]J. Putnam and J. Littell, "Simulation and analysis of NASA lift plus cruise eVTOL crash test," in *Vertical Flight Society's 79th Annual Forum* (Vertical Flight Society, 2023). https://ntrs.nasa.gov/citations/20230003711.
[68]J. Kim, S. Lee, and D. Im, "Conceptual design of two-seater lift & cruise type urban air mobility," in *AIAA SciTech 2024 Forum* (AIAA, 2024).
[69]J. C. Figueira, S. Bazzocchi, S. Warwick, and A. Suleman, "Nonlinear aero-propulsive modeling for fixed-wing eVTOL UAV from flight test data," J. Aircraft **62**(2), 300–312 (2025).
[70]A. Brown and W. L. Harris, "Vehicle design and optimization model for urban air mobility," J. Aircraft **57**(6), 1003–1013 (2020).
[71]A. Bacchini, E. Cestino, B. Van Magill, and D. Verstraete, "Impact of lift propeller drag on the performance of eVTOL lift+ cruise aircraft," Aerosp. Sci. Technol. **109**, 106429 (2021).
[72]Vertical Aerospace, "Vertical aerospace VX4." https://vertical-aerospace.com (accessed June 7, 2025).
[73]EHang, "EHang 216 eVTOL aircraft." https://www.ehang.com/ehangaav/ (accessed May 5, 2025).
[74]Volocopter, "Volocopter 2X." https://www.volocopter.com/en (accessed May 5, 2025).
[75]M. Ding, H. Li, L. Shao, J. Xuan, C. Feng, X. Yan, and D. Bie, "Evaluation of aerodynamic performance of a multi-rotor eVTOL during landing using the lattice Boltzmann method," Drones **9**(5), 332 (2025).
[76]Y. Yang, Y. Liang, S. Pröbsting, P. Li, H. Zhang, B. Huang, C. Liu, H. Pei, and B. R. Noack, "Sizing of multicopter air taxis—Weight, endurance, and range," Aerospace **11**(3), 200 (2024).
[77]Aquinea Volta eVTOL aircraft. https://aquinea.fr/helicoptere-electrique-volta/ (accessed May 5, 2025).
[78]C. Lim, J. Kim, J. Hong, S. Lee, and S. Lee, "The relationship between civil aircraft noise and community annoyance in Korea," J. Sound Vib. **299**(3), 575–586 (2007).
[79]J. Kim, "Urban air mobility noise: Further considerations on indoor space," Int. J. Environ. Res. Public Health **19**(18), 11298 (2022).
[80]Federal Aviation Administration. https://www.faa.gov (accessed May 11, 2025).
[81]European Union Aviation Safety Agency. https://www.easa.europa.eu/en (accessed May 11, 2025).
[82]Federal Aviation Administration, Code of Federal Regulations, Title 14—Aeronautics and Space, Part 36—Noise Standards: Aircraft Type and Airworthiness Certification. https://www.faraim.org/faa/far/cfr/title-14/part-36/index.html (accessed May 11, 2025).
[83]Federal Aviation Administration (FAA), "Integration of powered-lift: Pilot certification and operations; miscellaneous amendments related to rotorcraft and airplanes" (2024). https://www.federalregister.gov/citation/89-FR-92296 (accessed December 5, 2025).
[84]European Union Aviation Safety Agency (EASA), "Special condition for vTOL and means of compliance" (2025). https://www.easa.europa.eu/en/document-library/product-certification-consultations/special-condition-vtol (accessed December 5, 2025).
[85]M. Boucher, M. Rafaelof, D. Begault, A. Christian, S. Krishnamurthy, and S. Rizzi, "A psychoacoustic test for urban air mobility vehicle sound quality," SAE Int. J. Adv. Curr. Pract. Mobility **6**, 972–985 (2023).
[86]Matthew A. Boucher, Andrew W. Christian, Siddhartha Krishnamurthy, Tyler Tracy, Durand R. Begault, Kevin Shepherd, and Stephen A. Rizzi, "Toward a psychoacoustic annoyance model for urban air mobility vehicle noise," Technical Report NASA/TM-20240003202 (2024). https://ntrs.nasa.gov/citations/20240003202.
[87]S. Schade, R. Merino-Martinez, A. Moreau, S. Bartels, and R. Jaron, "Psychoacoustic evaluation of different fan designs for an urban air mobility vehicle with distributed propulsion system," J. Acoust. Soc. Am. **157**(3), 2150–2167 (2025).
[88]D. Casalino, W. C. van der Velden, and G. Romani, "Community noise of urban air transportation vehicles," in *AIAA SciTech 2019 Forum* (AIAA, 2019).
[89]S. A. Rizzi, D. L. Huff, D. D. Boyd *et al.*, "Urban air mobility noise: Current practice, gaps, and recommendations," Technical Report NASA/TP-20205007433 (2020).
[90]World Health Organization, *Guidelines for Community Noise* (World Health Organization, Geneva, 1999). https://www.who.int/publications/i/item/a68672 (accessed December 5, 2025).
[91]Airbus, Airbus reveals the next generation of CityAirbus. https://www.airbus.com/en/newsroom/press-releases/2021-09-airbus-reveals-the-next-generation-of-cityairbus (accessed May 11, 2025).
[92]Joby Aviation, "Joby confirms revolutionary low noise footprint following NASA testing" (2022). https://www.jobyaviation.com/news/joby-revolutionary-low-noise-footprint-nasa-testing/ (accessed June 30, 2025).
[93]A. Zanotti and D. Algarotti, "Aerodynamic interaction between tandem overlapping propellers in evtol airplane mode flight condition," Aerosp. Sci. Technol. **124**, 107518 (2022).
[94]R. de Vries, N. van Arnhem, T. Sinnige, R. Vos, and L. L. M. Veldhuis, "Aerodynamic interaction between propellers of a distributed-propulsion system in forward flight," Aerosp. Sci. Technol. **118**, 107009 (2021).
[95]R. E. Nargi, P. Candeloro, F. De Gregorio, G. Ceglia, and T. Pagliaroli, "Fluid-dynamic and aeroacoustic characterization of side-by-side rotor interaction," Aerospace **10**(10), 851 (2023).
[96]E. J. Alvarez, A. Schenk, T. Critchfield, and A. Ning, *Rotor-on-Rotor Aeroacoustic Interactions of Multirotor in Hover* (American Helicopter Society, 2020). https://par.nsf.gov/biblio/10316279.
[97]G. Qiao, T. Zhang, and G. N. Barakos, "Numerical simulation of distributed propulsion systems using CFD," Aerosp. Sci. Technol. **147**, 109011 (2024).
[98]W. Zhou, Z. Ning, H. Li, and H. Hu, "An experimental investigation on rotor-to-rotor interactions of small UAV propellers," in *35th AIAA Applied Aerodynamics Conference* (AIAA, 2017).
[99]C. Moreira, N. Herzog, and C. Breitsamter, "Wind tunnel investigation of transient propeller loads for non-axial inflow conditions," Aerospace **11**(4), 274 (2024).
[100]J. Li, H. Kwan Ng, Y. Zheng, and S. Gutierreznolasco, "Noise exposure maps for urban air mobility," in *AIAA Aviation 2021 Forum* (AIAA, 2021).
[101]W. Johnson, *Helicopter Theory* (Courier Corporation, 2012). https://aerocastle.wordpress.com/wp-content/uploads/2012/04/helicopter_theory.pdf.
[102]W. Johnson, "NDARC NASA design and analysis of rotorcraft," Technical Report NASA/TP-2015-218751 (2022). https://rotorcraft.arc.nasa.gov/Publications/files/Johnson%20TP-20220000355_v1.pdf.
[103]W. Froude, "On the elementary relation between pitch, slip, and propulsive efficiency," Technical Report NACA-TM-1 (1920). https://ntrs.nasa.gov/citations/19930080719.
[104]M. Felli, F. Di Felice, G. Guj, and R. Camussi, "Analysis of the propeller wake evolution by pressure and velocity phase measurements," Exp. Fluids **41**, 441–451 (2006).
[105]J. Susi, K.-E. Unt, and S. Heering, "Determining the efficiency of small-scale propellers via slipstream monitoring," Drones **7**(6), 381 (2023).
[106]Q. Huang, G. He, J. Jia, Z. Hong, and F. Yu, "Numerical simulation on aerodynamic characteristics of transition section of tilt-wing aircraft," Aerospace **11**(4), 283 (2024).
[107]P. Aref, M. Ghoreyshi, A. Jirasek, M. J. Satchell, and K. Bergeron, "Computational study of propeller–wing aerodynamic interaction," Aerospace **5**(3), 79 (2018).
[108]B. Ortun, R. Boisard, and I. Gonzalez-Martino, "In-plane airloads of a propeller with inflow angle: Prediction vs. experiment," in *30th AIAA Applied Aerodynamics Conference* (AIAA, 2012).
[109]A. Zanotti, A. Velo, C. Pepe, A. Savino, D. Grassi, and L. Riccobene, "Aerodynamic interaction between tandem propellers in eVTOL transition flight configurations," Aerosp. Sci. Technol. **147**, 109017 (2024).
[110]M. C. Stratton, "Empirical modeling of tilt-rotor aerodynamic performance," Master's thesis (Old Dominion University, 2021). https://digitalcommons.odu.edu/mae_etds/340/.
[111]R. J. Higgins, A. Zarev, G. N. Barakos, and R. B. Green, "Numerical investigation of a two-bladed propeller inflow at yaw," J. Aircraft **57**(2), 292–304 (2020).

[112]J. M. Seddon and S. Newman, *Basic Helicopter Aerodynamics* (John Wiley & Sons, 2011).
[113]W. Johnson, C. Silva, and E. Solis, "Concept vehicles for vTOL air taxi operations," Paper No. ARC-E-DAA-TN50731 (2018). https://ntrs.nasa.gov/citations/20180003381.
[114]C. Silva, W. R. Johnson, E. Solis, M. D. Patterson, and K. R. Antcliff, "vTOL urban air mobility concept vehicles for technology development," in *2018 Aviation Technology, Integration, and Operations Conference* (AIAA, 2018).
[115]R. C. Dingeldein, "Wind-tunnel studies of the performance of multirotor configurations," Report No. NACA-TN-3236 (1954). https://ntrs.nasa.gov/citations/19930083899.
[116]G. E. Sweet, "Hovering measurements for twin-rotor configurations with and without overlap," Report No. NASA-TN-D-534 (1960). https://ntrs.nasa.gov/citations/20040016423.
[117]M. Ramasamy, "Hover performance measurements toward understanding aerodynamic interference in coaxial, tandem, and tilt rotors," J. Am. Helicopter Soc. **60**(3), 1–17 (2015).
[118]H. Lee and D.-J. Lee, "Rotor interactional effects on aerodynamic and noise characteristics of a small multirotor unmanned aerial vehicle," Phys. Fluids **32**(4), 047107 (2020).
[119]E. J. Alvarez and A. Ning, "High-fidelity modeling of multirotor aerodynamic interactions for aircraft design," AIAA J. **58**(10), 4385–4400 (2020).
[120]S. Yoon, H. C. Lee, and T. H. Pulliam, "Computational analysis of multi-rotor flows," in *54th AIAA Aerospace Sciences Meeting* (AIAA, 2016).
[121]M. Veismann and M. Gharib, "High fidelity aerodynamic force estimation for multirotor crafts in free flight," in *AIAA SciTech 2020 Forum* (AIAA, 2020).
[122]R. Piccinini, M. Tugnoli, and A. Zanotti, "Numerical investigation of the rotor-rotor aerodynamic interaction for eVTOL aircraft configurations," Energies **13**(22), 5995 (2020).
[123]K. Combey, O. A. Elsayed, K. Qaissi, and M. Faqir, "Numerical analysis of multirotor aerodynamic interactions in one-after-another configuration," in *Delft International Conference on Urban Air Mobility, DICUAM, Delft, Netherlands* (TU Delft, 2024). https://cdn.aanmelderusercontent.nl/i/doc/31d62a2598dec71be8c2763b4713395f?forcedownload=True.
[124]J. Yin, F. D. Gregorio, K.-S. Rossignol, L. Rottmann, G. Ceglia, G. Reboul, G. Barakos, G. Qiao, M. Muth, M. Kessler *et al.*, "Acoustic and aerodynamic evaluation of DLR small-scale rotor configurations within GARTEUR AG26," CEAS Aeronaut. J. **16**, 1175–1196 (2024).
[125]A. Zanotti, A. Savino, D. Granata, L. Abergo, F. Caccia, A. Guardone, J. Yin, R. Wickersheim, M. Kessler, A. Visingardi *et al.*, "Acoustic and aerodynamic evaluation of POLIMI tandem propellers in hover and cruise flight conditions within GARTEUR AG26," CEAS Aeronaut. J. (2025).
[126]K. Combey, O. A. Elsayed, K. Qaissi, H. Chouiyakh, and F. Mustapha, "Numerical analysis of multirotor aerodynamic interactions in forward and transition flight," J. Aircraft (2025).
[127]D. Granata, A. Savino, D. Grassi, L. Riccobene, and A. Zanotti, "Aerodynamic and aeroacoustics investigation of tandem propellers in hover for eVTOL configurations," Aerosp. Sci. Technol. **155**, 109740 (2024).
[128]E. J. Alvarez and A. Ning, "Modeling multirotor aerodynamic interactions through the vortex particle method," in *AIAA Aviation 2019 Forum* (AIAA, 2019).
[129]D. Shukla and N. Komerath, "Multirotor drone aerodynamic interaction investigation," Drones **2**(4), 43 (2018).
[130]M. Veismann, C. Dougherty, and M. Gharib, "Effects of rotor separation on the axial descent performance of dual-rotor configurations," Flow **3**, E7 (2023).
[131]S. Chae, S. Lee, S. Hwang, S. Jeong, and J. Kim, "Effects of rotor–rotor interaction for a small tandem rotor operating in a crosswind," Phys. Fluids **36**(6), 065147 (2024).
[132]J. Ko and S. Lee, "Quantification of wake interaction effects on multi-rotor configurations in forward flight," Aerosp. Sci. Technol. **135**, 108188 (2023).
[133]M. Misiorowski, F. Gandhi, and A. A. Oberai, "Computational study on rotor interactional effects for a quadcopter in edgewise flight," AIAA J. **57**(12), 5309–5319 (2019).
[134]D. Barcelos, A. Kolaei, and G. Bramesfeld, "Aerodynamic interactions of quadrotor configurations," J. Aircraft **57**(6), 1074–1090 (2020).
[135]O. Pinti, A. A. Oberai, R. Healy, R. J. Niemiec, and F. Gandhi, "Multi-fidelity approach to predicting multi-rotor aerodynamic interactions," AIAA J. **60**(6), 3894–3908 (2022).
[136]R. Healy, F. Gandhi, and M. Mistry, "Computational investigation of multirotor interactional aerodynamics with hub lateral and longitudinal canting," AIAA J. **60**(2), 872–882 (2022).
[137]D. Witkowski, R. Johnston, and J. Sullivan, "Propeller/wing interaction," in *27th Aerospace Sciences Meeting* (AIAA, 1989).
[138]B. Mukherjee and K. Brentner, "Investigation of propeller-wing interaction noise and the potential contribution to eVTOL noise," in *Proceedings of the VFS Technical Conference on Aeromechanics Design for Transformative Vertical Flight, San Jose, CA, USA* (Vertical Flight Society, 2020), pp. 16–19.
[139]C. C. Paruchuri, D. C. Akiwate, S. Palleja-Cabre, A. Karimian, P. Joseph, and A. Parry, "Investigation into the mechanisms of propeller-wing interaction noise," in *28th AIAA/CEAS Aeroacoustics 2022 Conference* (AIAA, 2022).
[140]Z. Gao, H. Luo, X. Shao, D. Pan, L. Zeng, and L. Wang, "Meshless simulation of multi-propeller/wing interactions in typical distributed electric propulsion configurations," Aerosp. Sci. Technol. **163**, 110287 (2025).
[141]M. Firnhaber Beckers, M. Schollenberger, T. Lutz, D. Bongen, R. Radespiel, J. L. Florenciano, and D. E. Funes-Sebastian, "CFD investigation of high-lift propeller positions for a distributed propulsion system," in *AIAA Aviation 2022 Forum* (AIAA, 2022).
[142]D. Keller, "Aerodynamic investigation of the high-lift performance of a propeller-driven regional transport aircraft with distributed propulsion," J. Phys. Conf. Ser. **2526**(1), 012007 (2023).
[143]C. Xue and Z. Zhou, "Propeller-wing coupled aerodynamic design based on desired propeller slipstream," Aerosp. Sci. Technol. **97**, 105556 (2020).
[144]H. Aminaei, M. Dehghan Manshadi, and A. R. Mostofizadeh, "Experimental investigation of propeller slipstream effects on the wing aerodynamics and boundary layer treatment at low Reynolds number," Proc. Inst. Mech. Eng., Part G: J. Aerosp. Eng. **233**(8), 3033–3041 (2019).
[145]Y. Seo, Y. Hong, and K. Yee, "Numerical investigation of wing–multiple propeller aerodynamic interaction using actuator disk method," Int. J. Aeronaut. Space Sci. **23**(5), 805–822 (2022).
[146]J. C. Plijter, R. Duivenvoorden, and T. Sinnige, "Aerodynamic interaction effects between a propeller slipstream and single slotted flap," in *AIAA SciTech 2025 Forum* (AIAA, 2025).
[147]N. S. Zawodny, D. D. Boyd, and D. M. Nark, "Aerodynamic and acoustic interactions associated with inboard propeller-wing configurations," in *AIAA SciTech 2021 Forum* (AIAA, 2021).
[148]Y. Lei and X. Zhao, "Aerodynamic performance assessment of distributed electric propulsion after the wing trailing edge," Appl. Sci. **14**(1), 280 (2023).
[149]J. R. Serrano, A. O. Tiseira, L. M. García-Cuevas, and P. Varela, "Computational study of the propeller position effects in wing-mounted, distributed electric propulsion with boundary layer ingestion in a 25 kg remotely piloted aircraft," Drones **5**,56 (2021).
[150]R. d Vries, N. van Arnhem, F. Avallone, D. Ragni, R. Vos, G. Eitelberg, and L. L. M. Veldhuis, "Experimental investigation of over-the-wing propeller–boundary-layer interaction," AIAA J. **59**(6), 2169–2182 (2021).
[151]T. Sinnige, N. van Arnhem, T. C. A. Stokkermans, G. Eitelberg, and L. L. M. Veldhuis, "Wingtip-mounted propellers: Aerodynamic analysis of interaction effects and comparison with conventional layout," J. Aircraft **56**(1), 295–312 (2019).
[152]M. Minervino, G. Andreutti, L. Russo, and R. Tognaccini, "Drag reduction by wingtip-mounted propellers in distributed propulsion configurations," Fluids **7**(7), 212 (2022).
[153]A. Zanotti, L. Menini, A. Savino, D. Grassi, and L. Riccobene, "Experimental investigation of wing-propeller aerodynamic interaction in eVTOL configurations," Aerosp. Sci. Technol. **152**, 109348 (2024).
[154]H. E. Bloomer and N. E. Samanich, "QCSEE under-the-wing engine-wing-flap aerodynamic profile characteristics," Technical Report NASA-TM-82890 (1982). https://ntrs.nasa.gov/citations/19830003822.
[155]Ascendance Flight Technologies, "ATEA—Hybrid-electric vTOL aircraft" (2025). https://www.ascendance-ft.com/products/atea (accessed June 6, 2025).
[156]Y. Zhou, G. Huang, and C. Xia, "Analysis of fixed-wing vTOL aircraft with gas-driven fan propulsion system," Aerosp. Sci. Technol. **104**, 105984 (2020).
[157]Y. Zhu, G. Huang, C. Xia, and Y. Wu, "Aerodynamic design of fixed-wing vTOL aircraft powered by gas-driven fan propulsion system," Aerosp. Sci. Technol. **162**, 110165 (2025).

[158]B. Hoeveler, C. C. Wolf, M. Raffel, and F. Janser, "Aerodynamic study on efficiency improvement of a wing embedded lifting fan remaining open in cruise flight," in *2018 Applied Aerodynamics Conference* (AIAA, 2018).
[159]R. de Vries, T. Sinnige, and L. L. M. Veldhuis, "Aerodynamic performance and interaction effects of an over-the-wing distributed-propeller system in cruise conditions," in *34th Congress of the International Council of the Aeronautical Sciences* (ICAS, 2024). https://www.icas.org/icas_archive/icas2024/data/papers/icas2024_0632_paper.pdf.
[160]H. H. Hubbard, *Aeroacoustics of Flight Vehicles: Theory and Practice* (National Aeronautics and Space Administration, Office of Management, 1991). https://ntrs.nasa.gov/citations/19920001380.
[161]D. W. Kurtz and J. E. Marte, "A review of aerodynamic noise from propellers, rotors, and lift fans," Technical Report 32-1462 (1970). https://ntrs.nasa.gov/citations/19700005920.
[162]A. F. Deming, "Propeller rotation noise due to torque and thrust," J. Acoust. Soc. Am. **12**(1), 173–182 (1940).
[163]R. Schlinker and R. Amiet, "Helicopter rotor trailing edge noise," in *7th Aeroacoustics Conference* (AIAA, 1981).
[164]A. R. George and S. T. Chou, "Broadband rotor noise analyses," Report No. NASA-CR-3797 (1984). https://ntrs.nasa.gov/citations/19840014297.
[165]D. C. Akiwate, A. B. Parry, P. Joseph, and C. C. Paruchuri, "On the balance between the tonal and broadband noise of uninstalled propellers," in *AIAA Aviation 2021 Forum* (AIAA, 2021).
[166]G. Romani, E. Grande, F. Avallone, D. Ragni, and D. Casalino, "Computational study of flow incidence effects on the aeroacoustics of low blade-tip Mach number propellers," Aerosp. Sci. Technol. **120**, 107275 (2022).
[167]F. Yunus, D. Casalino, G. Romani, and M. Snellen, "Efficient prediction of propeller noise in non-axial uniform inflow conditions," Aerosp. Sci. Technol. **157**, 109860 (2025).
[168]A. David Thai, E. De Paola, A. Di Marco, L. G. Stoica, R. Camussi, R. Tron, and S. M. Grace, "Experimental and computational aeroacoustic investigation of small rotor interactions in hover," Appl. Sci. **11**(21), 10016 (2021).
[169]Z. Ning, "Experimental investigations on the aerodynamic and aeroacoustic characteristics of small UAS propellers," PhD thesis (Iowa State University, 2018). https://dr.lib.iastate.edu/entities/publication/5ba67388-b00a-4e5a-a7a9-4e5aeec957c7.
[170]G. Bernardini, F. Centracchio, M. Gennaretti, U. Iemma, C. Pasquali, C. Poggi, M. Rossetti, and J. Serafini, "Numerical characterisation of the aeroacoustic signature of propeller arrays for distributed electric propulsion," Appl. Sci. **10**(8), 2643 (2020).
[171]M. Roger and S. Moreau, "Tonal-noise assessment of quadrotor-type UAV using source-mode expansions," Acoustics **2**(3), 674–690 (2020).
[172]K. Pascioni and S. A. Rizzi, "Tonal noise prediction of a distributed propulsion unmanned aerial vehicle," in *2018 AIAA/CEAS Aeroacoustics Conference* (AIAA, 2018). https://ntrs.nasa.gov/citations/20190000886.
[173]K. A. Pascioni, S. A. Rizzi, and N. Schiller, "Noise reduction potential of phase control for distributed propulsion vehicles," in *AIAA SciTech 2019 Forum* (AIAA, 2019).
[174]B. Magliozzi, "Synchrophasing for cabin noise reduction of propeller-driven airplanes," in *8th Aeroacoustics Conference* (AIAA, 1983).
[175]J. F. Johnston, R. E. Donham, and W. A. Guinn, "Propeller signatures and their use," J. Aircraft **18**(11), 934–942 (1981).
[176]S. A. Rizzi, D. L. Palumbo, J. Rathsam, A. W. Christian, and M. Rafaelof, "Annoyance to noise produced by a distributed electric propulsion high-lift system," in *23rd AIAA/CEAS Aeroacoustics Conference* (AIAA, 2017). https://ntrs.nasa.gov/citations/20170005762.
[177]Z. Feng, T. Gan, V. T. Valente, K. S. Brentner, and E. Greenwood, "Broadband noise modulation of multirotor aircraft," J. Acoust. Soc. Am. **157**(2), 924–939 (2025).
[178]P. Joseph, P. Chaitanya, S. Elliott, M. Bhardwaj, and T. P. Chong, "Propeller tonal noise reductions through synchrophasing: Mechanisms and performance," J. Sound Vib. **610**, 119110 (2025).
[179]C. C. Paruchuri, P. Joseph, D. C. Akiwate, A. B. Parry, and S. D. Prior, "On the noise generation mechanisms of overlapping propellers," in *AIAA Aviation 2021 Forum* (AIAA, 2021).
[180]H. Bu, Z. Ma, and S. Zhong, "An experimental investigation of noise characteristics of overlapping propellers," J. Acoust. Soc. Am. **152**(1), 591–600 (2022).
[181]F. Caccia, L. Abergo, A. Savino, M. Morelli, B. Y. Zhou, G. Gori, A. Zanotti, G. Gibertini, L. Vigevano, and A. Guardone, "Multi-fidelity numerical approach to aeroacoustics of tandem propellers in eVTOL airplane mode," in *AIAA Aviation 2023 Forum* (AIAA, 2023).
[182]B. B. Turhan, H. Kamliya Jawahar, D. Rezgui, and M. Azarpeyvand, "Characterizing the noise patterns of overlapping propellers in forward flight," J. Acoust. Soc. Am. **157**(4), 2790–2801 (2025).
[183]Z. Jia and S. Lee, "Acoustic analysis of urban air mobility quadrotor aircraft," in *Vertical Flight Society (VFS) Aeromechanics for Advanced Vertical Flight Technical Meeting* (Vertical Flight Society, 2020), Vol. 38, pp. 14–15.
[184]A. Zarri, A. Koutsoukos, and F. Avallone, "Aerodynamic and acoustic interaction effects of adjacent propellers in forward flight," in *AIAA AVIATION 2023 Forum* (AIAA, 2023). https://arc.aiaa.org/doi/abs/10.2514/6.2023-4489.
[185]J. Sagaga and S. Lee, "Performance, aerodynamics, and aeroacoustics of side-by-side rotors using high-fidelity computational fluid dynamics," AIAA J. **61**(12), 5429–5445 (2023).
[186]J. Sagaga and S. Lee, "High-fidelity computational study of aerodynamic noise of side-by-side rotor in full configuration," J. Sound Vib. **592**, 118607 (2024).
[187]A. Celik, N. Syafiqah Jamaluddin, K. Baskaran, D. Rezgui, and M. Azarpeyvand, "Aeroacoustic performance of rotors in tandem configuration," in *AIAA Aviation 2021 Forum* (AIAA, 2021).
[188]A. Celik, N. Syafiqah Jamaluddin, K. Baskaran, S. Meloni, D. Rezgui, and M. Azarpeyvand, "Experimental characterisation of rotor noise in tandem configuration," Appl. Acoust. **222**, 110053 (2024).
[189]A. Zarri, F. d Prenter, F. Avallone, D. Ragni, and D. Casalino, "Effects of phase synchronization on the tonal sound directivity of distributed propellers," J. Acoust. Soc. Am. **157**(5), 3267–3281 (2025).
[190]B. Turhan, H. K. Jawahar, A. Gautam, S. Syed, G. Vakil, D. Rezgui, and M. Azarpeyvand, "Acoustic characteristics of phase-synchronized adjacent propellers," J. Acoust. Soc. Am. **155**(5), 3242–3253 (2024).
[191]M. Roger, "Aeroacoustic installation effects in propulsion systems," in *Enodise Lecture Series Measurement, Modelling and Simulations Techniques for Novel Aircraft Architectures*, edited by C. Schram and M. Roger (von Karman Institute for Fluid Dynamics, 2024). https://www.vki.ac.be/images/lectureseries/enodise/02_Roger.pdf.
[192]R. Wickersheim, M. Keßler, J. Sembowski, D. Bongen, and J. Gomes, "Numerical investigation and validation of noise sources of a distributed propulsion system," AIAA J. **63**, 1418–1430 (2025).
[193]D. C. Akiwate, A. Parry, P. Joseph, and C. C. Paruchuri, "Analytical investigation of propeller-wing interaction noise," in *28th AIAA/CEAS Aeroacoustics 2022 Conference* (AIAA, 2022).
[194]C. Paruchuri, S. Palleja-Cabre, P. Joseph, D. C. Akiwate, O. Westcott, and M. Ferraro, "Aeroacoustics source mechanisms of fixed-wing vTOL configuration," in *AIAA Aviation 2023 Forum* (AIAA, 2023).
[195]I. Zaman, M. Falsi, B. Zang, M. Azarpeyvand, and S. Meloni, "On the aeroacoustics of turbulent boundary layer ingesting propellers," Phys. Fluids **36**, 075172 (2024).
[196]F. Caccia, L. Galimberti, L. Abergo, A. Savino, A. Zanotti, M. Parsani, and A. Guardone, "Quasi-compact model for accurate noise prediction of complex rotor configurations," Appl. Acoust. **240**, 110928 (2025).
[197]Z. Cheng, F.-S. Lien, E. Yee, and H. Meng, "A unified framework for aeroacoustics simulation of wind turbines," Renewable Energy **188**, 299–319 (2022).
[198]S. Glegg and W. Devenport, *Aeroacoustics of Low Mach Number Flows: Fundamentals, Analysis, and Measurement*, 2nd ed. (Academic Press, Elsevier, 2023).
[199]J. E. F. Williams and D. L. Hawkings, "Sound generation by turbulence and surfaces in arbitrary motion," Philos. Trans. R. Soc. London Ser. A, Math. Phys. Sci. **264**(1151), 321–342 (1969).
[200]F. Farassat and G. P. Succi, "A review of propeller discrete frequency noise prediction technology with emphasis on two current methods for time domain calculations," J. Sound Vib. **71**(3), 399–419 (1980).
[201]R. K. Amiet, "Noise due to turbulent flow past a trailing edge," J. Sound Vib. **47**(3), 387–393 (1976).
[202]D. B. Hanson, "Helicoidal surface theory for harmonic noise of propellers in the far field," AIAA J. **18**(10), 1213–1220 (1980).

[203]L. LUO, X. Huang, and T. Zhang, "External and interior acoustics simulation for multi-propeller aircraft based on URANS+FW-H and acoustic-solid coupling," Chin. J. Aeronaut. **38**, 103453 (2025).
[204]E. Zwicker and H. Fastl, *Psychoacoustics: Facts and Models* (Springer Science & Business Media, 2013), Vol. 22.
[205]R. Merino-Martinez and L. N. Quaroni, "Human response to the noise emissions of an isolated propeller under turbulent inflow conditions," in *INTER-NOISE and NOISE-CON Congress and Conference Proceedings* (Institute of Noise Control Engineering, 2025), Vol. 272, pp. 2180–2191. https://research.tudelft.nl/files/254666677/4f502b21611842a78e1c.pdf.
[206]F. Casagrande Hirono, J. Robertson, and A. J. Torija Martinez, "Acoustic and psychoacoustic characterisation of small-scale contra-rotating propellers," J. Sound Vib. **569**, 117971 (2024).
[207]J. A. Torija, P. Chaitanya, and Z. Li, "Psychoacoustic analysis of contra-rotating propeller noise for unmanned aerial vehicles," J. Acoust. Soc. Am. **149**(2), 835–846 (2021).
[208]L. T. Silva, A. Magalhães, J. F. Silva, and F. Fonseca, "Impacts of low-frequency noise from industrial sources in residential areas," Appl. Acoust. **182**, 108203 (2021).
[209]K. Combey, H. Chouiyakh, K. Qaissi, M. Faqir, and O. A. Elsayed, "Aerodynamics investigation of novel toroidal joined blade tips propeller," in *Delft International Conference on Urban Air Mobility, DICUAM2024*, Delft, Netherlands (TU Delft, 2024). https://cdn.aanmelder-usercontent.nl/i/doc/faa8920ad13bb0a7ba1921c0254c35ed?forcedownload=True.
[210]Massachusetts Institute of Technology, "Toroidal propeller" (2022). https://www.ll.mit.edu/sites/default/files/other/doc/2022-09/TVO_Technology_Highlight_41_Toroidal_Propeller.pdf (accessed July 12, 2025).
[211]Y. Wei, F. Xu, S. Bian, and D. Kong, "Noise reduction of UAV using biomimetic propellers with varied morphologies leading-edge serration," J. Bionic Eng. **17**, 767–779 (2020).
[212]K. Qaissi, O. Elsayed, M. Faqir, and E. Essadiqi, "Aerodynamic optimization of trailing-edge-serrations for a wind turbine blade using Taguchi modified additive model," Energies **16**(3), 1099 (2023).
[213]H. M. Lee, Z. Lu, K. M. Lim, J. Xie, and H. P. Lee, "Quieter propeller with serrated trailing edge," Appl. Acoust. **146**, 227–236 (2019).